UNIVERSITÀ DEGLI STUDI DI PADOVA

DIPARTIMENTO DI FISICA E ASTRONOMIA "GALILEO GALILEI"

Corso di Laurea Magistrale in Fisica

New insights into the femtosecond to microsecond photoinduced dynamics of Pyrene and Indole

Candidato:
Mario Masetto
Matricola 1036308

Relatore:
Prof.ssa Cinzia Sada

Correlatori:
Prof. Eberhard Riedle
Dott. Igor Pugliesi

Anno Accademico 2013-2014

Index

1. Introduction

The progress in molecular biology relies partly on the deep insight into the molecular structure and processes that is offered by molecular physics, which in turn has experienced in the last decades a huge development thanks to the availability of fast computers, which allow for accurate calculations of potential energy surfaces, and new advanced experimental techniques. In this frame, electronic spectroscopy is gaining more and more importance, as it represents a versatile tool to investigate different energy scales and time domains, giving thus exhaustive information about the several steps and processes involved in a photoinduced chemical reaction.

The spectroscopy setup employed in this work permits to monitor, in a time resolved way, the evolution of a photoexcited chemical system, following its de-excitation dynamics. This is achieved by recording the transient absorption of the sample simultaneously over a broad spectral range, at different time intervals after the photoexcitation by an ultrafast pump pulse, fully tunable from the deep UV to the IR. This wide spectral coverage of both the pump and the probe, along with a time resolution of about 50 fs, proved of being able to provide unambiguous disentanglement of complex processes, as described in ref. [Rie13].

Here we investigate with these capabilities two well known “textbook” molecules: pyrene and indole. Both these aromatic molecules have significant relevance in molecular biology and their peculiar chemical and physical properties have been studied for decades; nevertheless, they present a rich and complex photodynamics on several time scales, many aspects of which have still to be clarified.

The interest in pyrene already began in the fifties, as soon as concentration dependent analysis of its fluorescence were performed and showed that pyrene emission displays a temporally delayed band in the blue whose intensity and decay time grow with increasing pyrene concentration. On this evidence, along with the absence of a concentration dependence of the absorption, the notion of eximer, i.e. a dimer that forms a bound state only in the excited state and dissociate into two monomers, was developed. This property made pyrene a useful fluorescent probe. Many adjustments have been made through the decades to the model for the excimer formation mechanism, that was first developed by Birks in 1963, in order to better interpret the time behaviour and the concentration dependence of pyrene emission, but

an unambiguous picture is still missing. Moreover, several theoretical and experimental studies supported the hypothesis of pre-association, i.e. the existence of pyrene ground state dimers. In the following we will show how evidence collected from ultrafast pump probe experiments can be crucial to the determination of the dimer formation mechanism.

The indole molecule is the chromophore of tryptophan, a common amino acid that absorbs in the UV, and is an excellent probe to monitor protein involving processes, thanks to its strong fluorescence. The structure of the fluorescence band and its spectral position as well as many other properties of indole and its compounds, are highly sensitive on the properties of the environment surrounding the molecule, in particular on its polarity. This can be very useful when dealing, for instance, with membrane proteins. The ultrafast nonradiative decays of indole then, like photoionization and internal conversion to the ground state, have been studied since they represent effective mechanisms to prevent damages by UV light to biological substances. Many of indole properties derive from the strong vibronic coupling between the two lowest $\pi\pi^*$ transitions and other dark excited states. In this thesis we will investigate, combining time-resolved and steady-state spectroscopy techniques, the complex interplay between these states, in relation to the de-excitation mechanisms of indole.

Chapter 2 of this work presents the basic concepts of transient spectroscopy and a brief description of the experimental setups we have used. In the chapters 3 and 4, we review the past studies about pyrene and indole, respectively, and we describe the results of our experimental analysis of the two molecules.

2. Experimental and interpretational methods

2.1 Ultrafast optical parametric amplification

The field of ultrafast optical science has witnessed great developments over the last two decades, thanks to the discovery of new materials and techniques, which made both ultrashort time scales and very high intensities easily accessible. One of these techniques is optical parametric amplification (OPA), which provides high output energies and a broad frequency tenability. OPA consists in the amplification, in a suitable nonlinear crystal such as β-barium borate (BBO), of a weak seed beam (called *signal*, at frequency ω_S) by a high intensity beam at higher frequency ω_P (called *pump*), with the collateral production of a third beam (called *idler*, at frequency ω_I, with $\omega_I<\omega_S<\omega_P$) dictated by energy conservation: $\hbar\omega_P = \hbar\omega_S + \hbar\omega_I$. A thorough review of ultrafast optical amplifiers can be found in ref. [Cer03]. In this section we will just summarise the most important features of the process.

In nonlinear crystals the nonlinear polarization conveys the interaction between different propagating waves and acts as a source term that drives the amplitude variations of the waves, so that an energy flow from the pump field to the two lower-frequency fields can take place. Crucial to the efficiency of the process is the fulfilment of the momentum conservation condition, also called phase matching:

$$\hbar\Delta\mathbf{k} = \hbar\mathbf{k}_P - \hbar\mathbf{k}_S - \hbar\mathbf{k}_I = 0$$

Phase matching can only be achieved in birefringent crystals, where the refractive index depends on the polarization direction. The condition, in fact, is equivalent to the relation: $n_P\omega_P = n_S\omega_S + n_I\omega_I$, where n is the refractive index. A way to match this relation consists in adjusting the angle θ between the wave vectors and the optical axis of the nonlinear crystal. The critical condition for obtaining ultrashort pulses is to broaden the spectral composition of the light, but a collinear phase matching is achieved only over a very restricted spectral range: the first order term in the power expansion of the wave vector mismatch Δk is proportional to the variation Δω of the signal frequency:

$$\Delta k \cong \left(1/v_{GI} - 1/v_{GS}\right)\Delta\omega$$

where the proportionality constant is the group velocity mismatch (GVM) between signal and

idler, $v_G = d\omega/dk$ being the group velocity of the pulse. This limitation sets a lower limit of about 50 fs to the obtainable pulse duration. Gale *et al.* [Gal95] found a solution to this problem by applying to the OPA the noncollinear geometry shown in Fig 2.1, i.e. by setting a suitable angle α between signal and pump wavevectors in the crystal.

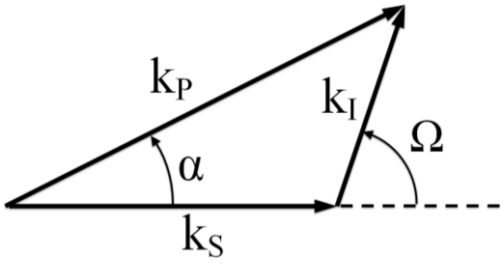

Fig 2.1 Noncollinear geometry for optical parametric amplification. α identifies the noncollinear angle between the signal and the pump wavevectors, whereas Ω is the angle formed by the signal and the resulting idler propagation directions.

The resulting angle Ω between signal and idler depends then on the frequency of the signal beam. With this setting the phase matching condition can be fulfilled at the first order of expansion if the following relation holds:

$$v_{GS} = v_{GI} \cos\Omega$$

that is, if the signal group velocity equals the projection of the idler group velocity along the signal direction. In this way the two beams manage to stay overlapped and efficiently interact while travelling through the crystal, and not to drift apart because v_{GI} is usually larger than v_{GS}. The consequence of choosing an angle α such that the previous relation is fulfilled, is that the angle θ that defines the phase matching becomes constant over an ultrabroad bandwith.

With noncollinear optical parametric amplification (NOPA) sub 20 fs pulses can be routinely obtained throughout all the visible range [Wil97]. All the details regarding the NOPA setup used for this thesis can be found in ref. [Rie00].

2.2 Transient spectroscopy

2.2.1 Basic concepts

Some of the major interests in the molecular dynamics field of study are the determination of

the energy surfaces of excited molecular states, the investigation of the behaviour of systems far away from equilibrium and of situations where the many approximations used in theory are set under stress. Transient absorption spectroscopy is an effective tool that has led and leads to ever deeper insight into these issues and into the disentaglement of complex processes that take part in molecular relaxation pathways after optical excitation [Rie13]. This technique is based on the simple fact that different intermediate states of a photoinduced reaction have different absorption bands. Detecting these bands in a time resolved way allows to follow the sequence of states populated by the photoproducts of excitation and at the same time to energetically characterize the states.

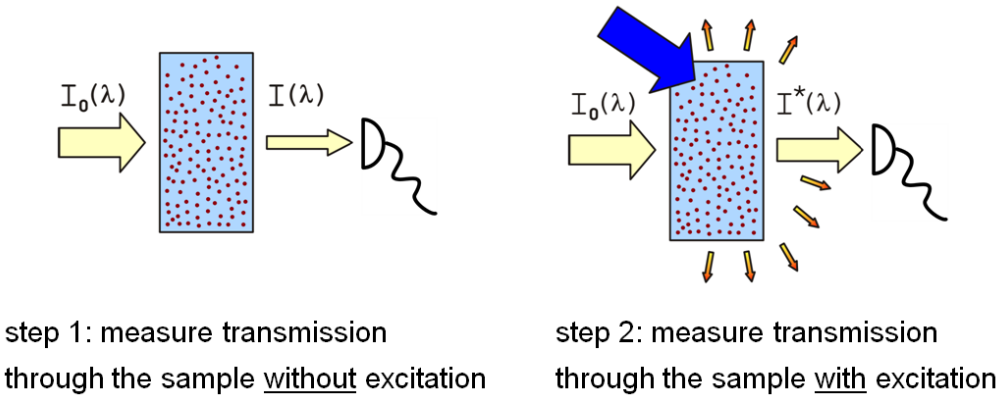

Fig 2.2 Illustration of a transient absorption experiment. $I_0(\lambda)$ is the incident intensity of the probe light, $I(\lambda)$ the transmitted intensity without excitation and $I^*(\lambda)$ is transmitted intensity through the excited sample (with courtesy of Christian Schriver).

In pump-probe transient spectroscopy, in order to extract the absorption spectrum of the excited states of a molecular system, the transmission of a probe laser pulse of intensity I_0 at a wavelength λ, both through the sample in its ground state ($T_0(\lambda)$)[1] and through the sample

[1] The transmission T is defined as the ratio of the intensity I of the light transmitted out of an irradiated sample and the intensity I_0 of the light falling upon the sample: $T = I/ I_0$. The optical density OD of the sample is then the opposite of the logarithm of transmission: $OD = - \log(T)$. This definition is in relation to the Beer-Lambert law, which states that the decrease in the intensity I over the course of a small volume element is proportional to the intensity of the light entering the element, the numerical concentration of absorbers (ρ), and the length of the path through the element (dx) [Par09]:

$$\frac{dI}{dx} = -\sigma\rho I \quad \rightarrow \quad I(x) = I_0 e^{-\sigma\rho x} = I_0 10^{-\varepsilon C x} \quad \rightarrow \quad OD(x) = \varepsilon\, C\, x$$

where C is the molar concentration, and the proportionality constant ε is called *molar extinction coefficient* (usually expressed in M^{-1} cm^{-1}) and depends on the wavelength of the incident light and on the nature of the absorber.

excited by a pump laser pulse ($T^*(\lambda,\Delta t)$, where Δt is the time interval between the pump and probe pulse incidences), are recorded. From these quantities the difference in the optical density is calculated:

$$\Delta OD(\lambda,\Delta t) = -\log\left[\frac{T^*(\lambda,\Delta t)}{T_0(\lambda)}\right]$$

This difference in the optical density is ascribed to the absorption properties of the transient states populated a time Δt after the excitation. A typical transient absorption (TA) spectrum is shown in Fig 2.3.

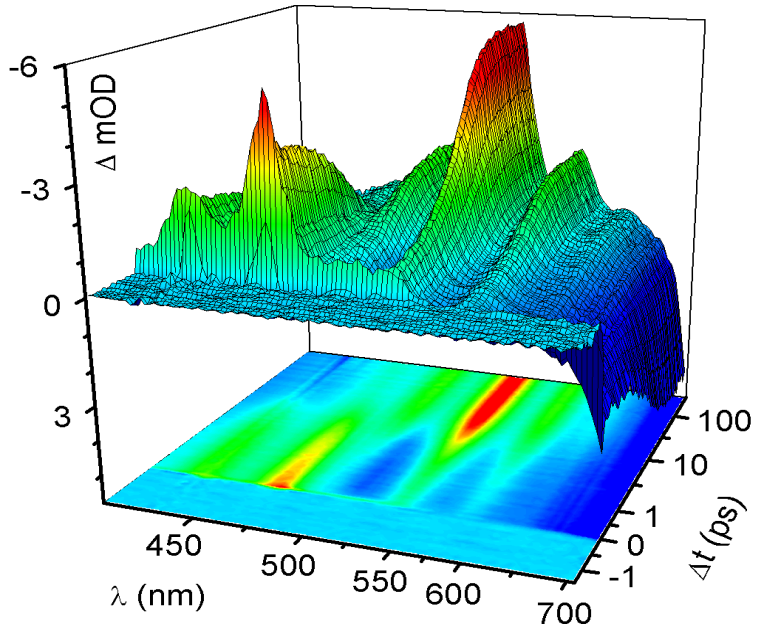

Fig 2.3 Typical transient absorption spectrum from a pump-probe measurement on a perylene diimide dyad (with courtesy of Igor Pugliesi).

There are three major contributions to TA spectra:

- Excited state absorption (ESA) and product absorption (PA): it is a positive signal (ΔOD > 0) corresponding to resonant transitions of the states that are populated after the optical excitation to even higher states or of products of chemical reactions possibly induced from photoexcitation.
- Ground state bleach (GSB): the increase in transmission, due to the fact that a fraction of the sample molecules have been excited and do not absorb from the ground state any more, leads to a negative contribution with the same features of the steady state absorption spectrum of the system. The GSB trace and its temporal behaviour give

then insight into the amount of molecules that populate the different excited states and the dynamics of the de-excitation to the ground state.

- Stimulated emission (SE): another negative signal comes from the emission from the excited states stimulated from the probe light, which resembles the steady state fluorescence spectra of the system.

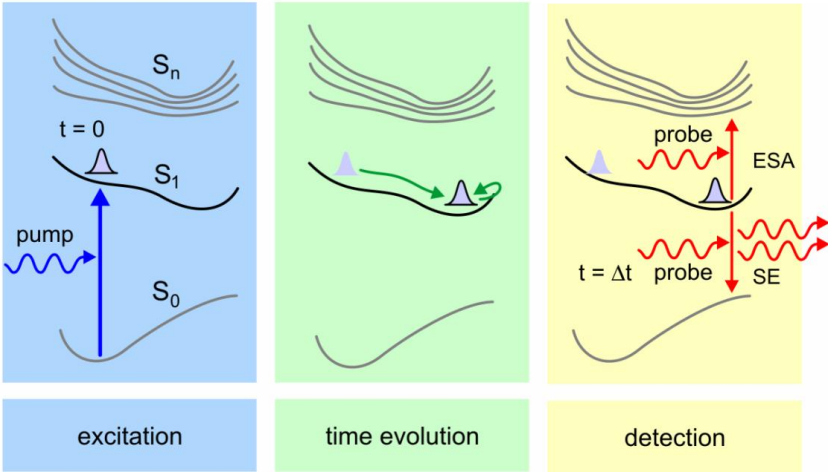

Fig 2.4 Schematic representation of the different contributions to TA signal (with courtesy of Christian Schriver).

The probability for a molecule in the sample to be excited from a laser pulse of energy E at a wavelength λ in a beam of diameter D, is given, as a first approximation, by the product of the photon density and the excitation cross section σ:

$$P_{exc} = n_{ph} \cdot \sigma = \frac{E}{\left(hc/\lambda\right)\pi\left(D/2\right)^2} \cdot \varepsilon \frac{10^3 \ln 10}{N_A}$$

where ε is the molar extinction coefficient of the absorbing species and N_A is the Avogadro number. The energy of the pump beam decreases while travelling through the sample following the Beer-Lambert law (if we neglect non-linear absorption processes, i.e. the simultaneous absorption of two or more photons by the same molecule):

$$E_P(\lambda_P, x) = E_P^0 e^{-\sigma_P \rho x}$$

with E_P^0 the energy of the pump pulse before hitting the sample, ρ the numerical concentration of pyrene molecules in the sample and σ_P the absorption cross section at the pump wavelength λ_P. If we then indicate with σ_i^* and σ_i^{SE} respectively the absorption and stimulated emission cross sections at the probe wavelength λ of an excited molecular state $|i\rangle$,

and with σ the absorption cross section of the ground state at λ, the three contributions to the TA signal can be expressed as follows:

- $\Delta OD_{ESA}(x,\lambda,\Delta t) = \frac{1}{\ln 10}\left[\sum_i \sigma_i^* p_i(\Delta t)\right] n_P^0 \left(1 - e^{-\sigma_P \rho x}\right)$
- $\Delta OD_{GSB}(x,\lambda,\Delta t) = -\frac{1}{\ln 10}\left[\sigma \sum_i p_i(\Delta t)\right] n_P^0 \left(1 - e^{-\sigma_P \rho x}\right)$
- $\Delta OD_{SE}(x,\lambda,\Delta t) = -\frac{1}{\ln 10}\left[\sum_i \sigma_i^{SE} p_i(\Delta t)\right] n_P^0 \left(1 - e^{-\sigma_P \rho x}\right)$

where $p_i(\Delta t)$ is the number of molecules populating the $|i\rangle$ state at the time Δt after the excitation divided by the total number of initial excited molecules. n_P^0 is the photon density in the pump pulse right before hitting the sample.

These components often overlap spectrally with each other and are modulated by additional effects due to the presence of the solvent in liquid solutions. Some reactions are driven or influenced by diffusion dynamics, whereas solute-solvent relaxation and solvation processes may cause time evolving spectral shifts of the absorption bands in the TA spectrum. Furthermore, non linear interactions between the pump and probe pulse in the region of their temporal overlap, due to the high pump power densities (typically > 10 GW/cm^2) required by the shortening of the pulse, overlap with the TA signal. The most significant among these interactions are two-photon absorption, stimulated Raman amplification and cross-phase modulation [Lor02]. Though these processes mask the signal and deteriorate the sensitivity right where the fastest molecular dynamics develops, their signature has also a positive effect, for each of them is produced by the simultaneous action of one photon of the pump and one of the probe resulting in a duration directly related to the temporal response function [Ras01]. From the so-called artifact, the temporal resolution of the experiment and the indication of the zero time of the dynamics can then be deduced.

2.2.2 Interpretation of TA spectra: the rate model

In order to extract significant information from the TA data, a reasonable model for the possible underlying molecular dynamics has to be assumed. The most basic approach to interpret the de-excitation reaction of a molecular system consists in describing the whole process as a sequence of specific intermediate steps and requiring, for each involved state, that the amount of population dN leaving the state in a small amount of time dt is proportional

to the current population N of the state: $dN/dt = -k\,N$, where k is the rate constant relative to the specific state. The system goes through a set of consecutive states, each one with a proper rate constant k, connected with the lifetime of the state $\tau = 1/k$.

As an example of such a model, consider a system that undergoes a three-step decay process (see Fig 2.5), after the instantaneous excitation at time t = 0 of all the molecules in the ground state: $N_0(t=0^-) = N_1(t=0^+) \equiv 1$.

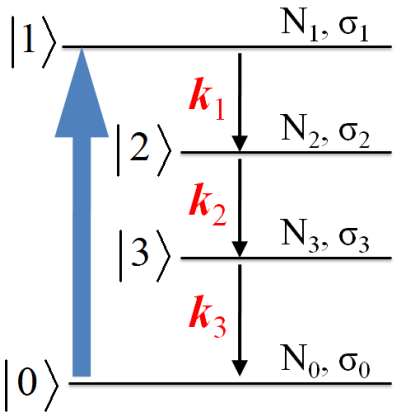

$$dN_1/dt = -k_1 N_1$$
$$dN_2/dt = k_1 N_1 - k_2 N_2$$
$$dN_3/dt = k_2 N_2 - k_3 N_3$$
$$dN_0/dt = k_3 N_3$$

Fig 2.5 Level diagram for a three-step decay process and differential equation for the population of the different states.

Integration of the rate equation in Fig 2.5 gives the following time behaviour for the population of the four states involved:

$$N_1 = e^{-k_1 t}$$
$$N_2 = \frac{-k_1}{k_1 - k_2} e^{-k_1 t} + \frac{k_1}{k_1 - k_2} e^{-k_2 t}$$
$$N_3 = \frac{k_1 k_2}{(k_1 - k_2)(k_1 - k_3)} e^{-k_1 t} + \frac{-k_1 k_2}{(k_1 - k_2)(k_2 - k_3)} e^{-k_2 t} + \frac{k_1 k_2}{(k_1 - k_3)(k_2 - k_3)} e^{-k_3 t}$$
$$N_0 = \frac{-k_2 k_3}{(k_1 - k_2)(k_1 - k_3)} e^{-k_1 t} + \frac{k_1 k_3}{(k_1 - k_2)(k_2 - k_3)} e^{-k_2 t} + \frac{-k_1 k_2}{(k_1 - k_3)(k_2 - k_3)} e^{-k_3 t} + 1$$

As explained in section 2.3.1, the transient absorption signal is proportional to the product of the population $N_i(t)$ of the $|i\rangle$ state and the state specific absorption cross-section spectra $\sigma_i(\lambda)$ (SAS); the difference in the optical density is then:

$$\Delta OD(\lambda,t) \propto \sigma_1(\lambda) N_1(t) + \sigma_2(\lambda) N_2(t) + \sigma_3(\lambda) N_3(t) + \sigma_0(\lambda)\left[1 - N_0(t)\right] =$$

$$= \left(\sigma_1 - \sigma_2 \frac{k_1}{k_1 - k_2} + \sigma_3 \frac{k_1 k_2}{(k_1 - k_2)(k_1 - k_3)} + \sigma_0 \frac{k_2 k_3}{(k_1 - k_2)(k_1 - k_3)} \right) e^{-k_1 t} +$$

$$+ \left(\sigma_2 \frac{k_1}{k_1 - k_2} - \sigma_3 \frac{k_1 k_2}{(k_1 - k_2)(k_2 - k_3)} - \sigma_0 \frac{k_1 k_3}{(k_1 - k_2)(k_2 - k_3)} \right) e^{-k_2 t} +$$

$$+ \left(\sigma_3 \frac{k_1 k_2}{(k_1 - k_3)(k_2 - k_3)} + \sigma_0 \frac{k_1 k_2}{(k_1 - k_3)(k_2 - k_3)} \right) e^{-k_3 t}$$

$$= A_1 e^{-k_1 t} + A_2 e^{-k_2 t} + A_3 e^{-k_3 t}$$

In this formulation each SAS is actually the difference between the ESA spectrum and the SE spectrum of the relative state, which makes $\sigma_0(\lambda)$ the steady state absorption spectrum of the system. The amplitudes A_i of the exponentials are called decay associated difference spectra (DADS) [Sto04] and can be directly estimated from the data by means of the fit procedures described in the following section. The knowledge of the DADS, along with that of the steady state spectra, allows to extract the absorption spectra of the states involved in the reaction chain.

2.2.3 Evaluation strategies for pump probe measurements

TA data collected from the measurements for this thesis consist of a matrix $\Delta OD_{ij} = \Delta OD(t_i, \lambda_j)$ where each row is a transient spectrum on a range of wavelength taken a certain delay time after or before the excitation. Data can be processed row by row or column by column or as a whole matrix, depending on the case. The different methods that have been used throughout this work are briefly described here.

- Single channel fit

  In order to have a first insight into the relevant time scales involved in the dynamics, the time evolution of the TA signal for single wavelength values is fitted, using a LabView routine, with the following function:

$$F(t) = IRF \otimes \left\{ \vartheta(t) \cdot \left[\sum_i A_i \exp\left(-t/\tau_i \right) + const \right] \right\} + artifact$$

  It consists of a superposition of exponentials, like what we expect from a rate model,

multiplied by the step function $\vartheta(t)$ and convoluted with the instrumental response function (IRF). The latter is given in pump-probe spectroscopy by the convolution of pump and probe pulses, which are assumed to be Gaussian, so that the IRF is a Gaussian too. The FWHM of the IRF gives an estimate of the time resolution of the experiment and is the lower limit for the time constants that can be reliably determined through the fit procedure. In addition to the smoothed exponentials, a Gaussian, with the same FWHM as the IRF, and optionally its derivatives are fitted to the data in order to model the coherent artifact arising from the nonlinear interaction between the pump and probe pulses in the sample.

The number of exponentials used to fit the transients is chosen according to the model used for the interpretation, if available, and so that the off-diagonal elements of the correlation matrix between the fit parameters do not approach ± 1. This last criterion assures that no excess parameters are used and prevents compensation effects in the fit that could alter the determination of the rate constants.

- Global fit analysis

  TA spectra are often affected by band shifts due to solvation effects or thermal relaxation processes and cannot be properly reproduced by a simple rate model such as the one described in sec. 2.3.2. This leads to local inconsistencies of the parameters obtained through single channel fits. Similar problems arise when fitting multi-exponential decay dynamics with time constants that are close together: in this case the estimated fit parameters present high correlations and differ significantly from the actual rate constants. A way to overcome these difficulties is offered by a global fit routine, described in details in ref. [Fit06], which can be applied to matrix data sets from TA experiments and consists of a simultaneous fit of the time traces at all wavelengths with one common set of rate parameters. Through the minimization of a χ^2 function in the space of the time constants, the routine finds an optimal set for their values as well as for the decay associated difference spectra corresponding to those decays.

2.2.4 Pump probe setup

The following briefly describes the experimental setup used to investigate the transient absorption signal in the laboratories of the Chair for BioMolecular Optics at LMU, Munich. More details can be found in ref. [Meg09].

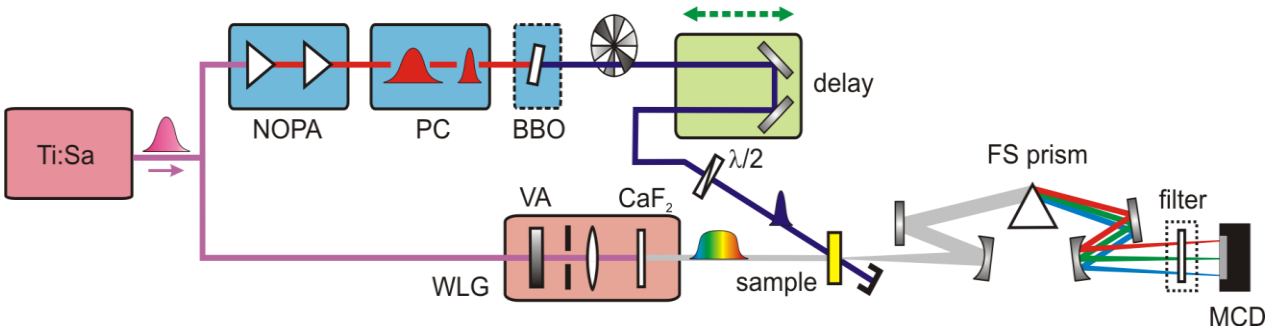

Fig 2.6 Schematic illustration of the pump-probe experiment setup for investigating ps scale dynamics (with courtesy of Uwe Megerle, [Meg11b] Figure 2.2).

The system is powered by a regenerative Ti:Sa amplifier (CPA 2001; ClarkMXR) that delivers 1 mJ-pulses at 775 nm with 150 fs duration and a repetition rate of 1 kHz. The beam is split and a fraction of 200–250 µJ enters a two-stage noncollinearly phase-matched optical parametric amplifier (NOPA, see sec. 2.1), giving as output a chirped visible pulse with energies of several µJ which is compressed with a sequence of two Brewster prisms. In order to adjust the pulse energy to the needs of the experiment, a thin achromatic half-wave plate permits to rotate the polarization and a wire-grid polarizer (ProFlux™; MOXTEK, Inc.) regulates the transmitted energy. Subsequently, the visible pulses are frequency doubled in a type-I BBO crystal, so that UV pulses can be obtained. The time interval between pump and probe pulses is then determined with a retro reflector mounted on a computer controlled linear stage. The pump beam is then focused on the sample. Another half-wave plate directly before the sample allows to set the polarization of the pump beam. The typical diameter of the beam at the sample position varies between 100 and 150 µm FWHM, according to the excitation probability needed in the experiment.

The probe pulse is generated by focusing 1 µJ of the fundamental beam into a CaF_2 crystal. This yields a chirped white light pulse, whose spectrum extends from 290 nm to 720 nm (see Fig 2.7), with an energy density of about 10 pJ/nm. The beam is focused on the sample and

passes through it at an external angle of ~6° with respect to the pump, overlapping the pump beam at the sample position, where the diameter of the probe is about 30 μm. The probe beam is then recollimated, dispersed through a fused silica prism polychromator and focused onto a multichannel detector (a back-thinned full frame transfer CCD camera, triggered synchronously to the laser).

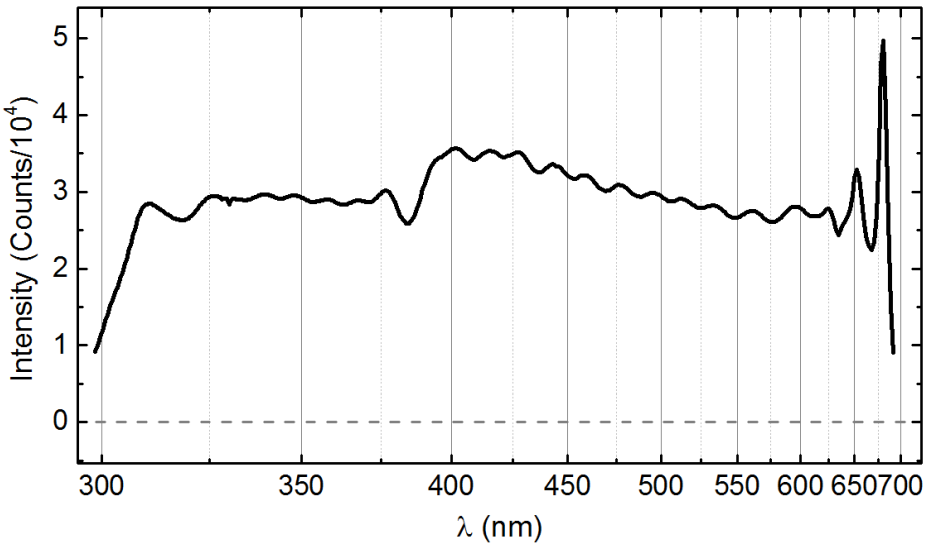

Fig 2.7 Spectrum of the white light continuum, used as probe beam for TA measurements, generated in CaF_2, as recorded by the CCD camera.

A chopper wheel running at half the laser repetition rate is inserted in the pump beam path in order to block every second excitation pulse so that changes in the optical density of the sample can be easily measured by referencing the absorption of one probe pulse to the absorption of the next (see sec 2.3.1). This method for measuring the induced absorption change relies on the high correlation of successive probe pulses.

The delay between pump and probe can vary from Δt = -0.1 ns to about 1.7 ns. This interval is divided so that an equal weight is given to different time scales: the step size is chosen constant between -1 and 1 ps and is then linearly increased according to:

$$\Delta t(i) = \begin{cases} -1 + 2i / N & \text{for } i = 0,...,N-1, \\ 10^{-1+i/N} & \text{for } i = N,...,M. \end{cases}$$

where N is the number of points between -1 and 1 ps and $M = N(1+\log \Delta t_{\max})$.

The sample solution can be contained in a conventional stationary glass cuvette, in a special custom-made flow cell [Meg09] with 200 μm fused silica windows, or in a liquid jet [Tau03].

In each case the sample holder can be moved in three dimensions through a fine regulation in order to properly adjust the sample with respect to the spatial overlap of pump and probe beams. An effort to limit the thickness of the glass windows and the sample aims to reduce the coherent artifact, which masks the very fastest molecular signatures. After the prism compression, pump pulse durations below 30 fs are routinely achieved throughout the visible, resulting in an overall time resolution for the TA signal below 50 fs while using a flow cell with a 100 μm sample thickness.

One striking aspect of the setup described above is the possibility of substituting the excitation beam coming from the NOPA with the beam coming from an OPO operated with a diode-pumped Nd:YAG laser (EKSPLA^{NT} 242), which delivers ~3 ns pulses tunable from 210 to 2600 nm (see Fig 2.8). This modification extends the range for the delay time of the measured transients up to milliseconds, giving thus the possibility to explore processes happening on the ns time scale, like fluorescence or intersystem crossing to triplet state and many other de-excitation ractions. In this case the time delay between pump and probe is not generated in a mechanical way as in the ps setup, but through an electronic delay generator which triggers the OPO and synchronizes it to the fs Ti:Sa laser used for the probe with a precision below 200 ps.

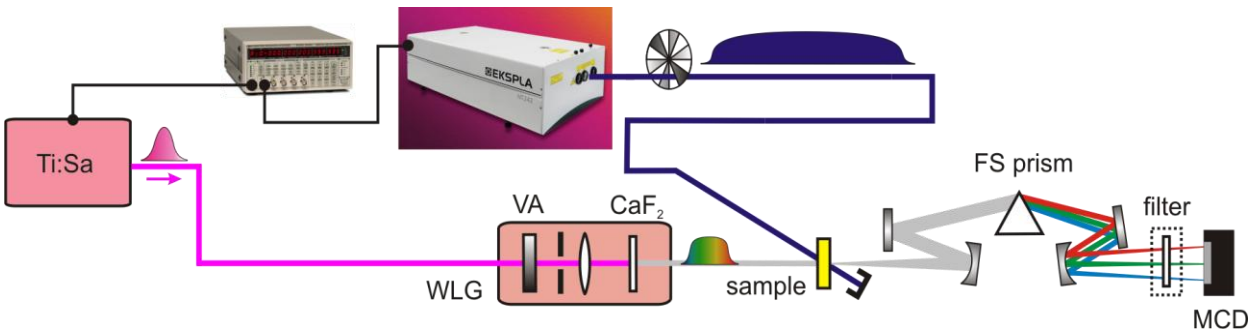

Fig 2.8 Schematic illustration of the pump-probe experiment setup for investigating ns scale dynamics (with courtesy of Uwe Megerle).

2.3 Fluorescence spectroscopy

2.3.1 Basic concepts

Steady state and time resolved fluorescence spectroscopy have been major tools in biochemistry and biophysics research for decades [Lak06]. They offer deep insight into the vibrational structure of molecular levels of aromatic molecules, as well as into de-excitation processes, and have been widely used as detection procedures both in science and in industrial and technical applications.

"Fluorescence" describes the spontaneous emission of light from an electronically excited system, whose wavefunction has the same spin multiplicity of the ground state molecular orbital, which is a singlet state for most of organic molecules. The transition is then spin allowed, contrary to the slower intersystem crossing from a singlet to a triplet state, and the emission rates are typically about 10^8 s^{-1}, which results in a lifetime on the 10 ns time scale. In the vast majority of cases the decay takes place from the lowest energy vibrational level of the S_1 state (the so called Kasha's rule [Kas50]) and ends on the higher vibrational levels of the S_0, even if the system had been previously excited to higher levels, since the internal conversion from those states to the thermally equilibrated S_1 happens much faster than fluorescence (typically on the ps time scale). For this reason the fluorescence spectrum gives a picture of the vibrational structure of the ground state orbital S_0. Furthermore, since electronic excitation does not significantly modify the nuclear positions so that the vibrational structure of S_1 and S_0 are similar, the fluorescence spectrum mirrors the absorption. As can be easily derived from a Jablonski diagram, fluorescence occurs at lower energies than absorption; this redshift of fluorescence is called Stokes shift (see Fig 2.9).

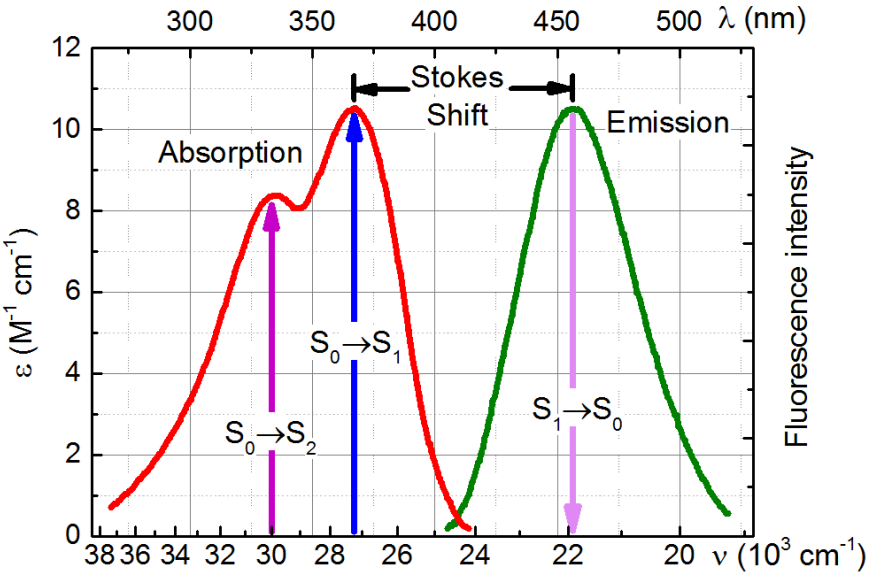

Fig 2.9 Quinine absorption and emission spectra, with indication of the Stokes shift. Quinine is a widely encountered fluorophore, present e.g. in tonic water, which is excited by UV light and fluoresces in the blue. Data taken from [Lak06].

2.3.2 Setup for time resolved fluorescence spectroscopy

During the work for this thesis a simple setup for measuring time resolved fluorescence on the ns to µs time scale has been developed. This is schematically represented in Fig 2.10.

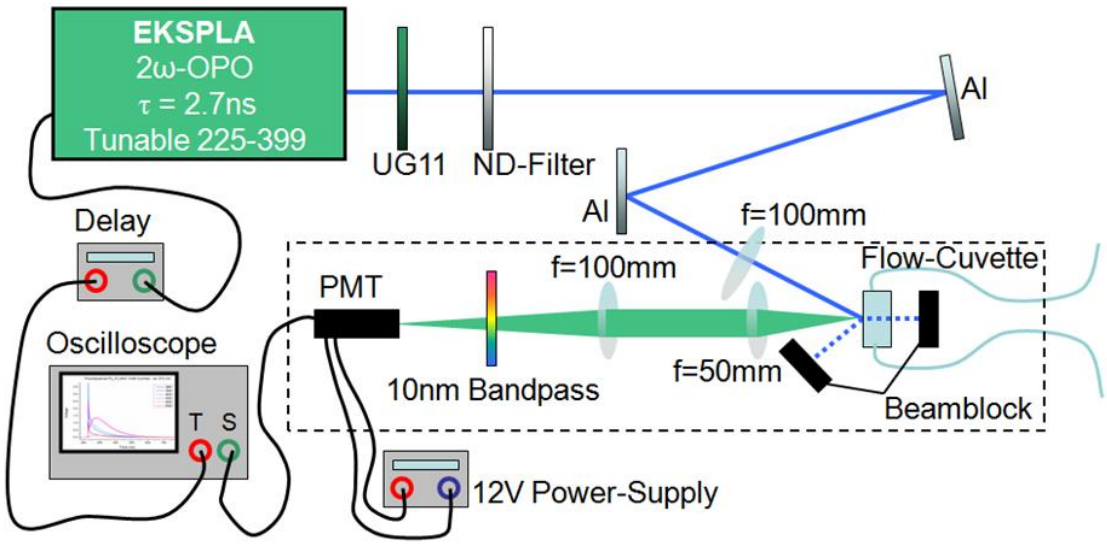

Fig 2.10 Schematic illustration of the setup for investigating time-resolved fluorescence emission (figure by Bastian Baudisch).

A wavelength tunable beam from an OPO (EKSPLA^{NT} 242) is focused with a 10 cm fused silica lens onto a flow cell containing the sample solution. A UG11 filter is placed in the beam path in order to suppress the fundamental 532 nm light of the Nd:YAG laser pumping the OPO, subsequently a neutral density filter is used to adjust the intensity of the light pulse to the needs of the experiment.

Front face fluorescence emission is collected by a 5 cm lens, thus collimated, and then focused by another lens on a photomultiplier tube. Different 10 nm bandpass filters can be placed in front of the photomultiplier (PMT, HAMAMATSU H5783) to select the desired detection-wavelength from the fluorescence emission. Sample cell, light collecting optics and PMT are contained in a black box to minimize optical noise. The PMT signal is directly viewed via an oscilloscope (YOKOGAWA DL9040, 5 GS/s, 500MHz). The trigger signal for the oscilloscope is synchronized with the laser and conveniently delayed through an electronic delay generator. Finally the time trace recorded by the oscilloscope can be saved as an ASCII file.

With the above described setup, we were able to record, with a time resolution of about 3 ns, the time behaviour of pyrene fluorescence emission, as described in sec. 3.6.

3. Pyrene: a textbook molecule with some major surprises

3.1 Introduction to the molecule

Pyrene ($C_{16}H_{10}$) is a prototypical molecule of the polycyclic aromatic hydrocarbons (PAHs) group, and it consists of four fused benzene rings, resulting in a flat aromatic system (Fig 3.1). Pyrene and its derivatives have been widely used in various applications in biophysics [Han13], and their fluorescence emission has been extensively studied both in condensed phase, in solution and in supersonic jets. Pyrene has been applied as a fluorescent probe due to the long lifetimes, distinguishable and microenvironment dependent emission and high fluorescence quantum yields [Ber10, Fig11, Bir70], for instance, as a sensor incorporated in membranes and for monitoring protein structures and conformations [Pen02, Bai11], or to probe solvent polarities [Rei94].

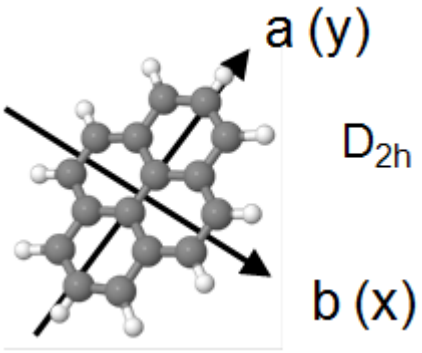

Fig 3.1 Illustration of pyrene molecular structure.

Pyrene photoinduced dynamics has revealed a particularly complex nature from the fs to the μs timescale, which made it a major subject of both theoretical and experimental studies in the last half century [Bir75, Win93, Par06, Kre13]. Continuous wave spectra show distinct electronic absorption bands, each modulated by the vibrational structure (Fig 3.2). The transition from the ground state S_0 ^1A_g to the first excited state S_1 $^1B_{3u}$ has a very weak absorption compared to the transitions to higher electronic states (e. g. S_2 $^1B_{2u}$) because it is forbidden due to the symmetry of the states [Bab09]. Nevertheless, the steady state emission originates from S_1 state, since strong vibronic couplings of electronic states ([Dei71]) leads to a very fast internal conversion (IC) from the higher states to S_1, with a time constant smaller

than 150 fs [Neu99, Ray03]. It has recently been demonstrated that the IC happens as a ballistic vibrational wavepacket motion through the $S_2 - S_1$ conical intersection and the wavepacket finally oscillates in the S_1 state; the IC process conserves the impulse of the nucleic motion excited in the S_2 and leads to nucleic motion in the S_1 state with the respective vibrational modes [Kre13]. After the IC, the vibrational excess energy in the S_1 state is redistributed along the vibrational S_1 modes in about 2 ps and the vibration relaxation to the S_1 vibrational ground state happens with 4.7 ps [Neu99, Kre13].

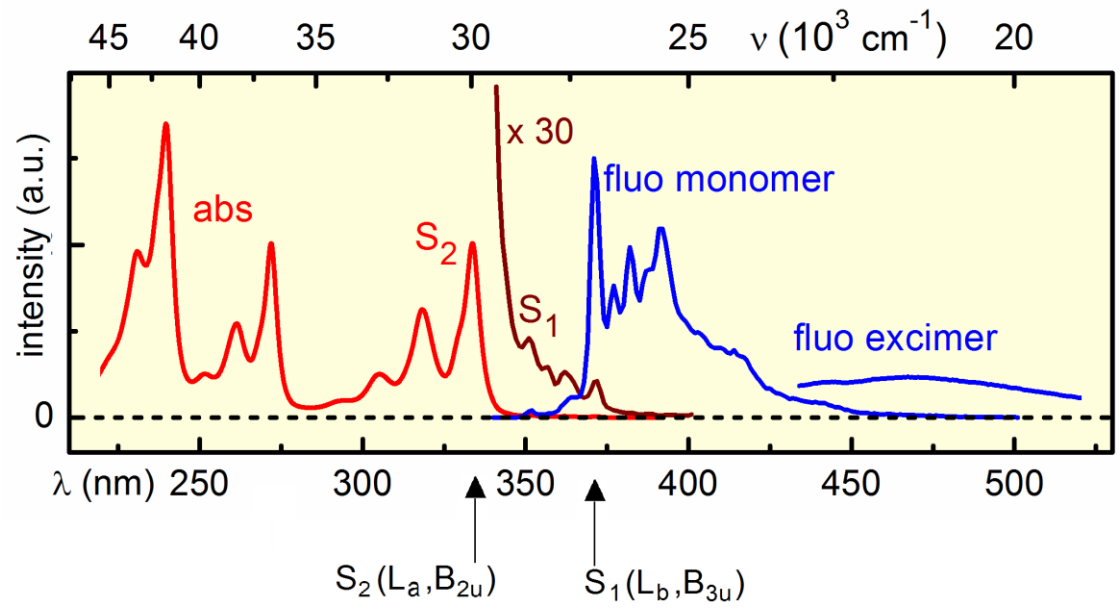

Fig 3.2 Fluorescence (blue line) and absorption (red line) spectra of pyrene in solution. The signature of the vibrational structure is clear to see. The absorption of the S_1 state has been multiplied by 30 times (brown line) in order to see its structure.

3.2 Properties of Pyrene fluorescence

At low concentrations pyrene molecule exhibits a well structured fluorescence band in the UV and violet, which shows the usual mirror symmetry to the absorption spectrum. In 1955, Förster and Kasper first observed that this band is replaced at higher concentrations by a structureless emission in the blue (Fig 3.3), whereas there is no change in the absorption spectrum within the corresponding concentration range [Foe55]. They also discovered that the dependence of the fluorescence on the concentration is affected by the solvent viscosity. From this all they deduced that the UV and violet band is emitted by the singlet excited pyrene

molecule, and the blue component is emitted by excited dimers. These are created as transients, from pairs of excited and unexcited monomers in diffusion controlled processes.

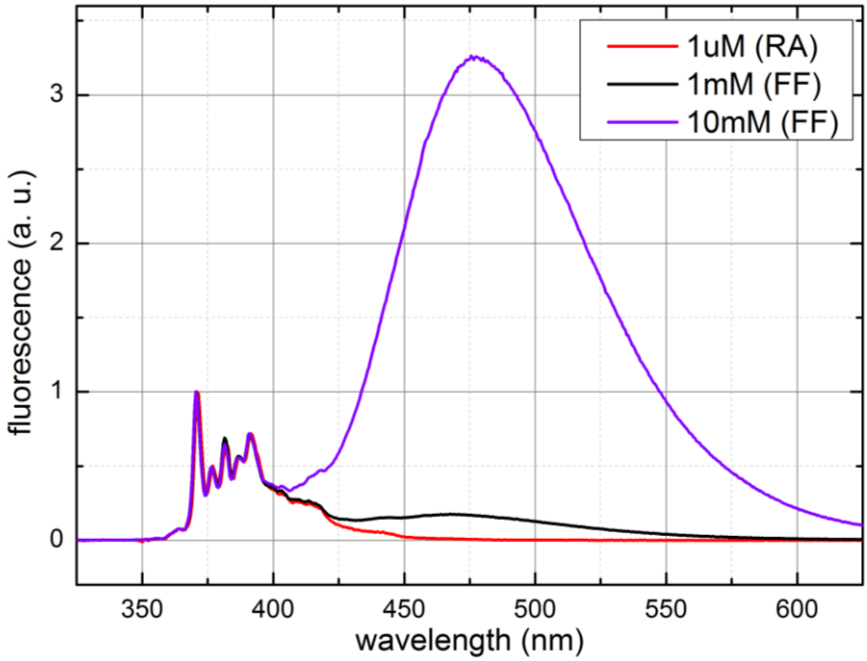

Fig 3.3 Fluorescence spectra of pyrene in methanol solution at various concentrations after excitation at 318 nm. As the concentration is increased, an unstructured band in the blue rises. Measurement by Elias Eckert.

The two fluorescence bands showed particularly long lifetimes and, in 1960, Stevens and Hutton suggested the term 'excimer' be used to distinguish the blue-emitting species in pyrene solution from the short-living dimer excited directly in solutions exhibiting an absorption spectrum dependent on concentration. The lack of an absorption trace of the excimer had been previously accounted as a crucial proof for the absence of a ground state dimer. Stevens and Hutton argued though that, since the radiative transition between excited and unexcited state is in the case of dimers optically forbidden if the complex has a centre of symmetry (which accounts for the magnitude of the excimer radiative lifetime), the corresponding absorption would be extremely difficult to detect even if the dimer exists to an appreciable extent in its ground state [Ste60].

In 1963, Birks *et al.* studied the concentration dependence of the monomer and excimer fluorescence of deoxygenated solution of pyrene in cyclohexane, after excitation with a ~ 10 ns pulse from a hydrogen lamp. They gave the first full kinetic treatment of the pyrene excimer [Bir63]: the experimental data were found to be consistent with a six rate parameters

reaction scheme, composed of the following processes:

Process	Description	Rate parameter (s^{-1})
• $Py^* \rightarrow Py + h\upsilon_M$	fluorescence of Py*	$k_{f\,M}$ } k_M } X
• $Py^* \rightarrow Py$	internal quenching of Py*	$k_{i\,M}$ }
• $Py^* + Py \rightarrow Ex^*$	excimer formation	$k_{EM}\,c$ }
• $Ex^* \rightarrow Py + Py + h\upsilon_E$	fluorescence of Ex*	$k_{f\,E}$ } k_E } Y
• $Ex^* \rightarrow Py + Py$	internal quenching of Ex*	$k_{i\,E}$ }
• $Ex^* \rightarrow Py^* + Py$	regeneration of Py* from dissociation of Ex*	k_{ME} }

where we indicated with Py the pyrene monomer, with Ex the excimer, and with c the concentration of pyrene molecules. The rate parameters are grouped as shown. It was de facto assumed a pseudo-first order kinetics ([Py*] « [Py]) and that the excimer formation rate is directly proportional to the pyrene concentration.

Assuming a δ-function at time $t = 0$ as excitation pulse, double exponential equations are derived for the time dependence of the pyrene singlet excited state and pyrene excimer concentrations:

$$\frac{[Py^*]}{[Py^*]_0} = \frac{\lambda_2 - X}{\lambda_2 - \lambda_1} e^{-\lambda_1 t} + \frac{X - \lambda_1}{\lambda_2 - \lambda_1} e^{-\lambda_2 t} \equiv \frac{\lambda_2 - X}{\lambda_2 - \lambda_1} \left(e^{-\lambda_1 t} + A e^{-\lambda_2 t} \right)$$

$$\frac{[Ex^*]}{[Py^*]_0} = \frac{k_{EM} c}{\lambda_2 - \lambda_1} \left(e^{-\lambda_1 t} - e^{-\lambda_2 t} \right)$$

where $\lambda_{1,2} = \frac{1}{2} \left[X + Y \pm \sqrt{(Y - X)^2 + 4 k_{ME} k_{EM} c} \right]$ are the roots of the differential equations that describe the reaction scheme, and $[Py^*]_0$ is the concentration of excited pyrene monomers at time $t = 0^+$.

The equations predict that the monomer fluorescence undergoes a double exponential decay, for the factor A is always positive, whereas the signal from the excimer rises with the time constant $\tau_2 = 1/\lambda_2$ and decays with $\tau_1 = 1/\lambda_1$. The rate parameters k_M, k_{EM}, k_E and k_{ME}, could be evaluated from measurement of λ_1 and λ_2 as a function of the concentration c, whereas $k_{f\,M}$, $k_{i\,M}$, $k_{f\,E}$ and $k_{i\,E}$ could be determined from k_M and k_E thanks to the measurement of the fluorescence quantum yields of the two species.

In this way Birks *et al.* could obtain an estimate of all the six parameters of the model,

choosing them so that the theoretical curves for λ_1 and λ_2 (see Fig 3.4) gave the best fit to the experimental data. These values are:

- $k_{f\,M} = 1.5\times10^{6}\,s^{-1}$; $k_{i\,M} = 7.88\times10^{5}\,s^{-1}$
- $k_{f\,E} = 1.16\times10^{7}\,s^{-1}$; $k_{i\,E} = 3.88\times10^{6}\,s^{-1}$
- $k_{ME} = 6.5\times10^{6}\,s^{-1}$; $k_{EM} = 6.7\times10^{9}\,M^{-1}s^{-1}$

A particularly high fluorescence quantum yield was reported, namely 0.75 for the excimer and 0.65 for the monomer. Interesting was that the values of k_{EM} closely agreed with those of κ, the theoretical molecular collision rate parameter [Bir63], which lead to the conclusion that the excimer formation is a diffusion-controlled collision process, and that every collision between Py* and Py is effective.

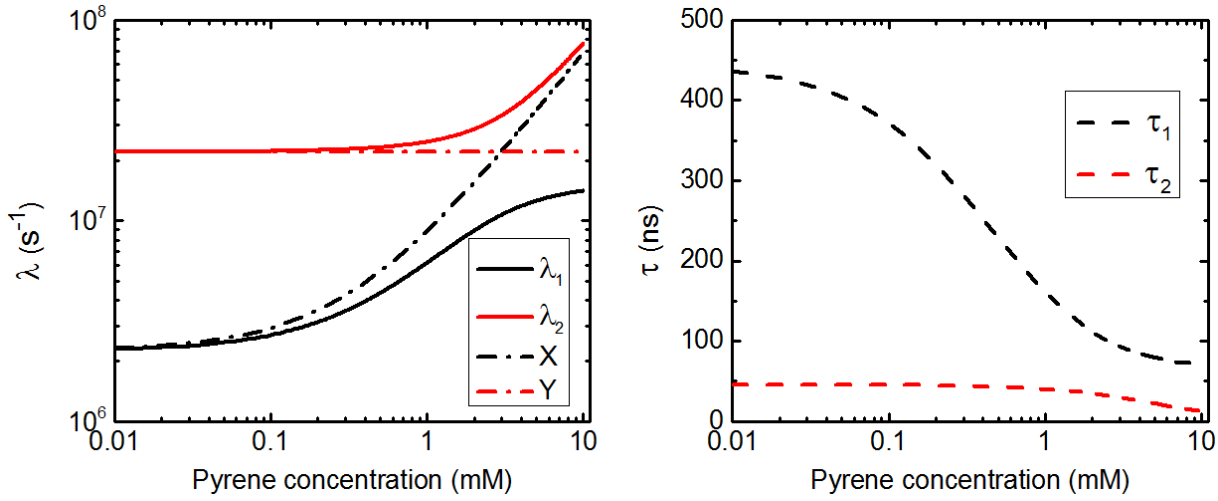

Fig 3.4 Concentration dependence of the rate and time constants according to Birks' model.

Up to a certain concentration c_A, dependent on the temperature (c_A ~ 2mM at T = 293K), the monomer fluorescence was found to correspond to a simple exponential decay of decay constant λ_1. This is in accordance with the analytic solution of the differential equation (Fig 3.5), which predicts small values of the coefficient A at low concentrations (A < 0.2 for c < 1 mM at 293K), i.e. for those concentrations the monomer fluorescence shows a monoexponential decay, with the same decay constant with which the excimer fluorescence decays.

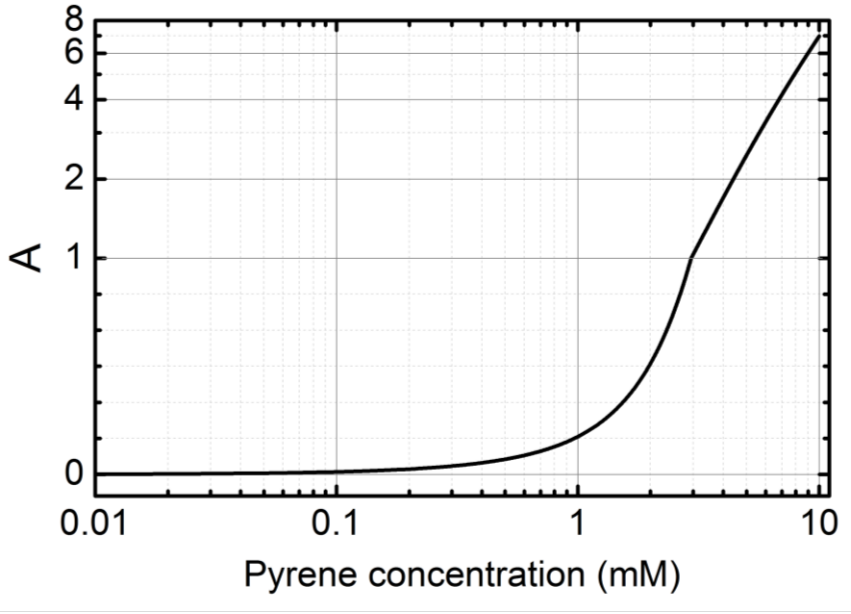

Fig 3.5 Dependence of the A coefficient in Birks' model on pyrene concentration at 293K.

Note that the introduction of the possibility for the excimer to generate a Py* and a Py modifies the dynamics description of the system. When excluding this process the monomer decay becomes strictly monoexponential and the roots of the differential equations are simply X and Y (see also Fig 3.4):

$$\frac{[Py^*]}{[Py^*]_0} = e^{-X\,t}$$

$$\frac{[Ex^*]}{[Py^*]_0} = \frac{k_{EM}c}{Y-X}\left(e^{-X\,t} - e^{-Y\,t}\right)$$

The work of Birks served as a reference model for every subsequent investigation on pyrene fluorescence. Very recently, Hanlon and Milosavljevic [Han13] have stressed the inconsistencies present in various reaction schemes used to interpret pyrene excimer formation in the past half century. In particular, they accused the scarcely coherent use of the k_{ME} parameter, which describes the dissociation of the excimer to give a ground state and an excited monomer, and the still not clear time dependence of k_{EM} [Mar92]. In their work they faced the problem of the concentration gradient of the excited monomer within the sample cell, consequent to the excitation. They claimed that pseudo-first order kinetics cannot be applied if the usual excitation to the first vibrational band of S_2 state (λ = 337 nm) is

employed, since the big molar extinction coefficient at this wavelength ($\varepsilon(337\text{nm}) = 3.4\times10^4 M^{-1}cm^{-1}$ for pyrene in decane) leads to a very high concentration gradient of both the excited and ground state pyrene molecules, which determines singlet-singlet annihilation, second order kinetics, non homogeneous diffusion and more artifact in the data. This is, in their opinion, the major issue that has affected studies using high concentrations of pyrene and excitation wavelength less than 350 nm. To avoid this problem, they chose to directly excite the S_1 state, which, due to the unfavourable symmetry properties, has a much lower ε ($\varepsilon(366\text{nm}) = 156\ M^{-1}cm^{-1}$ for pyrene in decane), resulting into simple homogeneous kinetics, which means a first order decay of the monomer fluorescence.

While comparing the fluorescence emission after excitation at 366 nm and at 337 nm, Hanlon and Milosavljevic underlined the experimental evidence that even using a low energy pulse at 337 nm (i.e. exciting only a few molecules), the monomer emission remains a multi-exponential decay and does not approach the monoexponential signal obtained after excitation at 366 nm. They deduced that the difference can be attributed to the excited pyrene concentration gradient, which only depends on the absorbance at the excitation wavelength and cannot be altered by varying the laser beam intensities.

The first order nature of the decay observed at 366 nm indicates also that the contribution of k_{EM} is negligible. This is moreover confirmed by energetic considerations: the binding energy of the excimer is reported to be of the order of 1 eV [Hue08, Shi11], that is much greater than k_BT (= 0.025 meV at 25°C). This makes highly unlikely that solvent molecules with enough energy to cause dissociation will collide with the excimer during its lifetime.

Finally, Hanlon and Milosavljevic found out that not every collision between singlet excited state and ground state pyrene molecules is effective in forming an excimer (approximately 40% of collisions were estimated to be effective at 25°C) and following temperature dependence related arguments, they stated that excimer formation is driven by conformational requirements and that the energy of activation for this process has a negative value (E_A = -11.2 ± 0.5 kJ mol^{-1}), which may be attributed to steric effects in the collision of the reactants.

The estimates for the rate parameters that they found for pyrene in decane solution at 25°C are:

- $k_{fM} + k_{iM} = (2.38\pm0.01)\times10^6 s^{-1}$
- $k_{fE} + k_{iE} = (2.78\pm0.02)\times10^7 s^{-1}$
- $k_{EM} = (3.11\pm0.06)\times10^9 M^{-1}s^{-1}$

3.3 Pre-association issue

Most of the works about pyrene, like the one from Birks, exclude the existence of pyrene ground state dimers, mainly because of the absence of such a trace in absorption spectra. Nevertheless, there have been several studies claiming the presence of ground state dimers of pyrene or pyrene derivatives in solutions and in other organized media [Bir75, Kha01, Win93].

In 1965 excimer emission was detected from pyrene solutions in cyclohexane which had been quickly frozen to 77 K, even for low pyrene concentrations (10^{-5}M) [Fer65]. Since excited monomers could not diffuse in the crystal to form excimers, such emission was attributed to ground-state dimers present in the solutions and trapped by the freezing.

Andriessen at al. demonstrated the existence of ground-state dimers of pyrene in cyclohexane at room temperature with various methods, namely the quantum yield measurements of an excimer-forming solution quenched by iodomethane, the compartmental analysis of fluorescence decay traces at different pyrene concentrations and the study of the ratio of fluorescence intensities at the monomer and excimer emission bands as a function of excitation wavelength [And92]. In particular, thanks to the second method they were able to estimate the equilibrium constant K for the dimer-forming process, that is the ratio between the concentration of the ground-state dimers and the square of the monomer concentration at equilibrium: $K = (2.45 \pm 0.01) \times 10^3$ M^{-1}. From this value, the relative concentration of monomers and ground-state dimers with respect to the total concentration c of pyrene in cyclohexane solution can be calculated (Fig 3.6); at c = 1mM, for instance, about half of the pyrene molecules is aggregated in dimers, which means that preassociation could really have a major role in pyrene photodynamics.

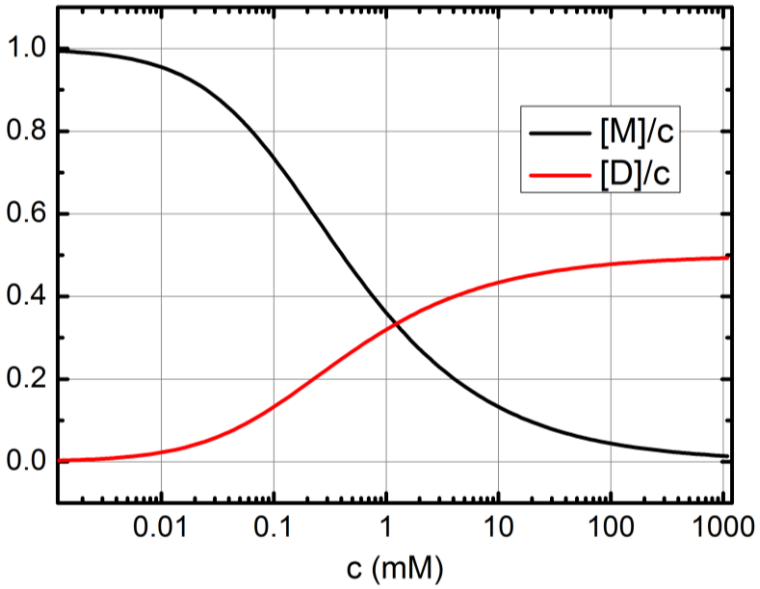

Fig 3.6 Concentration of monomers [M] and ground-state dimers [D] as a function of total pyrene concentration c, according to [And92].

Computations based on density functional theory integrated with empirical correction for long-range dispersion effects (namely a sum of damped atomic potentials of the form C_6R^{-6}) were applied to the study of the ground-state dimers of several aromatic molecules [Gri04]. According to these studies an isolated pair of pyrene molecules stacked on one another in a parallel displaced configuration makes a stable complex, bound with an energy of about 0.5 eV [Hue08], much bigger than the thermal energy (26 meV at room temprature).

Shirai et al. have recently performed calculations of the electronic states of pyrene dimer, both in the excited and in the ground-state configuration, using multiconfiguration quasi-degenerate perturbation theory [Shi11]. Since the excimer is the lowest among the excitonic states of the S_2 state of the monomer (L_a in Platt notation [Pla49]), in these studies the excimer is described with electron configurations built from the interaction between the frontier molecular orbitals (HOMO and LUMO) used to model the excitations to the S_2 state of two pyrene monomers. Shirai et al. were able to calculate the potential energy curves as function of the intermolecular distance for the excited and ground-state dimers, finding a minimum in both cases. The attractive interaction in the excited state turned out to be much stronger than in the ground state and the red-shift of the excimer fluorescence from the mirror image of the absorption spectrum was explained by the observation that the minimum of the excited-state curve is located in the repulsive region of the ground-state curve. In the picture of this paper the role of the ground-state dimer is that of a possible decay product of the

excimer. The mixing of excitonic-resonance (ER) states and charge-resonance (CR) states is known to contribute to the attractive interaction in aromatic excimers [Azu64, Azu64b, Mur64]. Such mixing gets stronger for short intermolecular distances, and near the minimum of the excimer energy curve the contribution of CR is almost equivalent to that from the ER. In Shirai's work, dispersion forces (i.e. instantaneous dipole-induced dipole forces) are taken into account through the perturbation calculation and represent the predominant force responsible for the binding interaction of the ground-state dimer.

The theoretical studies just mentioned dealt with molecules in vacuum conditions. The effects of the solvent may though play an important role in the dimerisation since the solvation energy of two monomers is larger than that of a dimer, and have been often accounted for discrepancies between theoretical estimates and experimental values. For this reason we have studied the photodynamics of electronically excited pyrene in solvents with different polarities, namely cyclohexane, tetrahydrofurane and methanol.

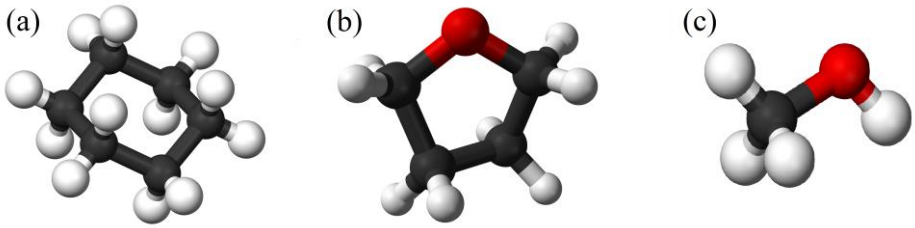

Fig 3.7 Schematic representation of the molecular structure of the employed solvents: cyclohexane (a), THF (b) and methanol (c).

Pyrene is a non-polar molecule, dissolution should then be enhanced in non-polar solvent (as can be seen from the solubility values reported in the following table) whereas dimer formation should be more likely in polar solvents, since solvation energy plays a smaller contribution.

Solvent	Stat. diel. const.	Pyrene solubility
Cyclohexane	2	0.100 M
THF	7.5	0.150 M
Methanol	32.6	0.036 M

Table 3.1 Values of the dielectric constant were taken from [Wik01], of solubility from [Acr02].

3.4 Short time dynamics

In order to investigate the ultrafast dynamics of the excited pyrene molecule we used the fs-spectroscopy setup described in section 2.2.4, with the pyrene solution flowing in a 100 µm cuvette. We used several pump wavelengths: we excited the molecule in the S_2 state, in its first, second or third vibrational band, i.e. at 334 nm, 318 nm and 305 nm wavelength respectively. Measurements have been carried out by Elias Eckert and Nils Krebs [Kre13].

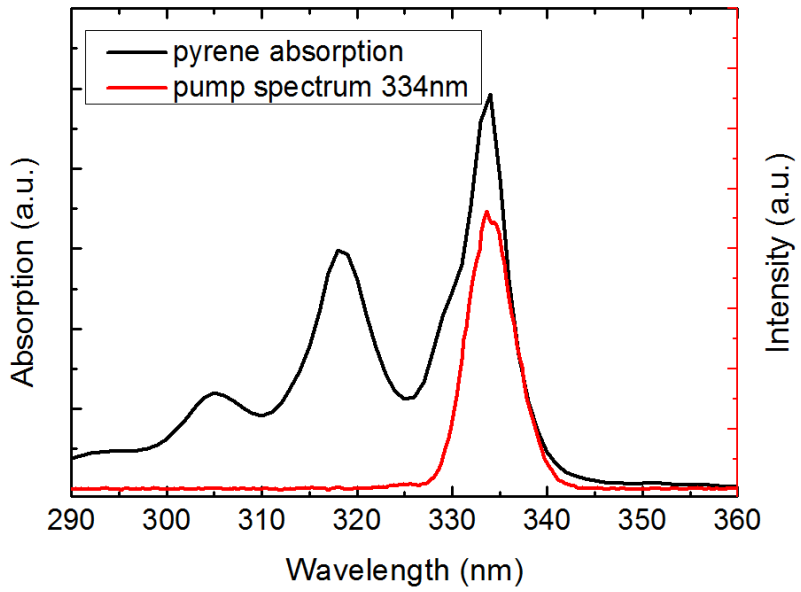

Fig 3.8 Absorption of pyrene S_2 state and example of a spectrum of the pump pulse (334 nm).

The errors on the estimated time constants that we will report in the following, both in this chapter relative to pyrene and in the next one relative to indole photodynamics, have been determined as the deviation of the fitted constants resulting from a set of measurements (at least three) that have been recorded with the same experimental conditions.

In Fig. 3.9 the first nanosecond of the transient absorption measurement of pyrene in methanol (1 mM) after excitation to the lowest vibrational level of the S_2 state is shown.

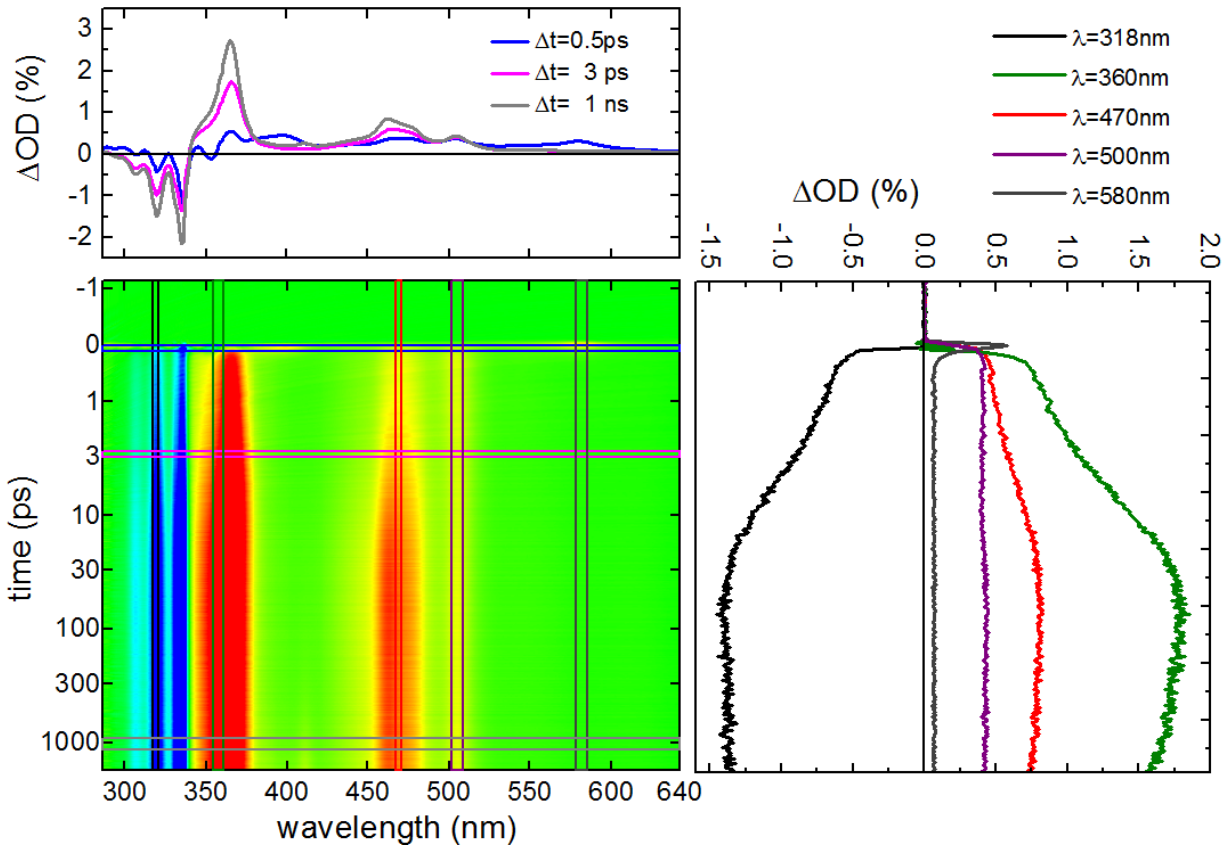

Fig 3.9 TA spectrum and profiles of a 1mM solution of pyrene in methanol after excitation at 334 nm.

Between 290 and 340 nm the signature of the ground state bleach (negative signal) with the characteristics of the S_2 state absorption spectrum is clear to see. Rapidly vanishing absorption contributions are visible at 400 and 580 nm and can be fitted with a (85 ± 20) fs exponential decay, which value is actually very close to the temporal resolution of the experiment (about 75 fs) and in excellent agreement with the results of [Ray03]. A wide, long living absorption between 340 and 550 nm, with two broad major peaks at 370 and at 470 nm, appears with the same 85 fs, grows exponentially in (6.6 ± 0.5) ps and decays on the ns time scale. Literature reports attribution of a 585 nm band to the $S_{14} \leftarrow S_2$ transition [Neu99], and the absorption between 370 and 470 nm resembles very well the reported absorption from the S_1 state [Fog95, Neu99], therefore we can state that after the excitation to the S_2 state the molecule undergoes an ultrafast internal conversion to the S_1 state, where a redistribution of the internal vibrational energy occurs and the vibrational relaxation is completed in the first 10 ns.

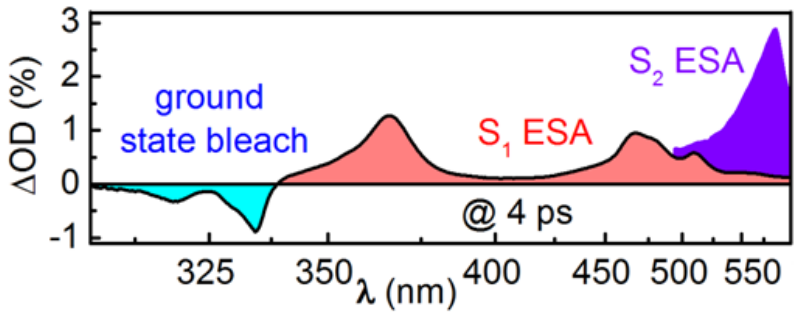

Fig 3.10 Interpretation for the different contributions to the transient absorption of pyrene in methanol, from a high-temporal resolution transient pump-probe experiment, performed with 310 nm excitation and parallel polarization between pump and probe pulses.

A striking aspect of the presented pump-probe spectrum is the decrease (increase in absolute value) of the signal in the region of the ground state bleach. The absorption diminishes by about a factor 2.5 of the initial value at $\Delta t = 200$ fs, with a time constant similar to that of the vibrational relaxation in the S_1 state. This signature of the GSB could be attributed to a decrease in the S_1 ESA that overlaps the GSB, motivating thus the time behavior. In order to verify this hypothesis the absorption spectrum of pyrene has been subtracted from the GSB in the transient spectra before and after the decrease of the signal. The result is shown in Fig 3.11.

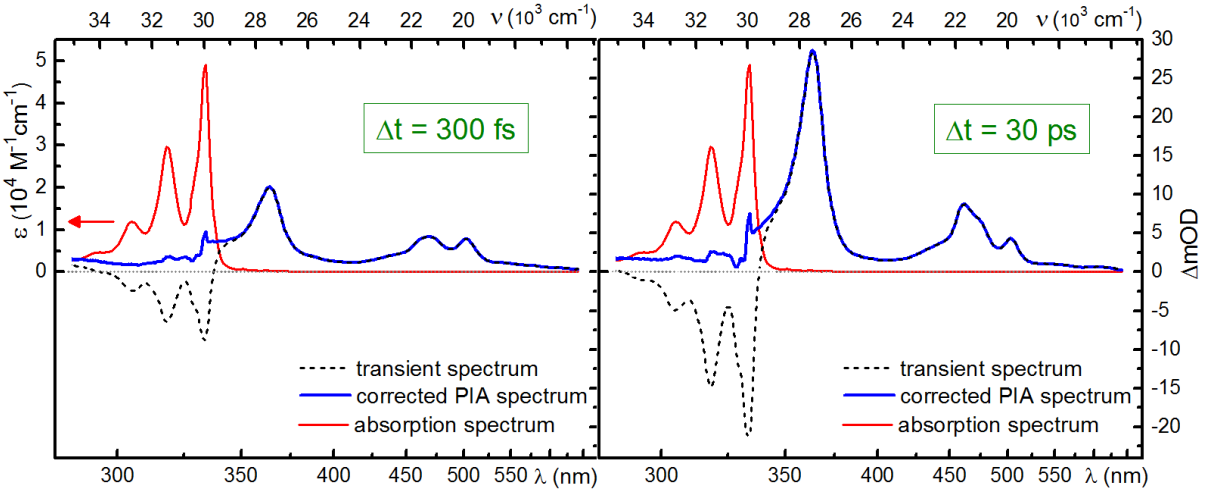

Fig 3.11 Subtraction of the properly scaled absorption spectrum from the GSB in the TA signal before and after the increase of the GSB.

As can be seen, there is no significant difference in the photo-induced absorption (PIA)

resulting from the subtraction in the two cases. There is no sign of an adequate absorption contribution that overlaps the GSB and decays within 30 ps. The only changing trace in the region between 290 and 340 nm is the one of the GSB. Another important aspect regarding the GSB is the dependence of the dynamics on the excitation wavelength. As shown in Fig 3.12, while the behavior of the PIA is not affected by the excitation wavelength, the increase of the bleach vanishes as we excite higher vibrational levels of the S_2 state, i. e. with more vibrational energy in the S_1 state right after the IC.

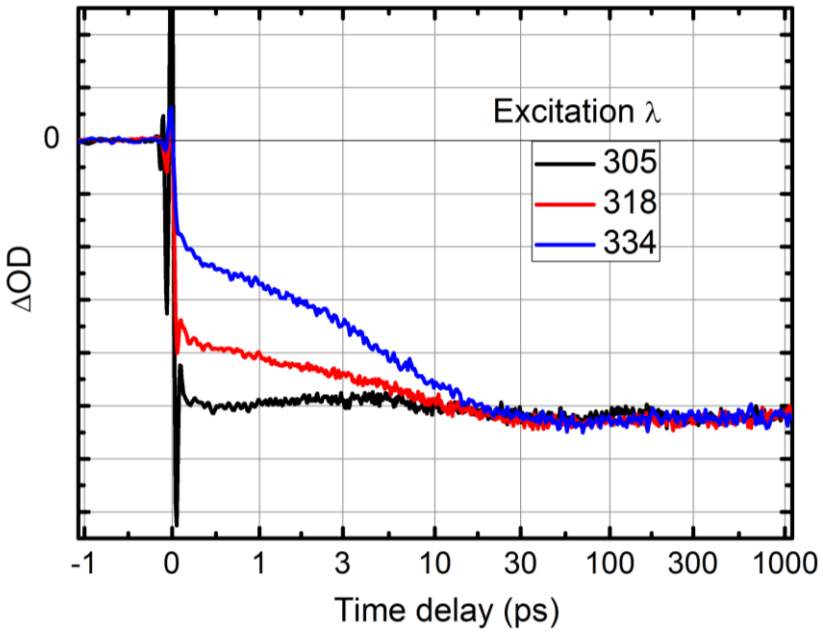

Fig 3.12 Time trace of TA at λ = 318 nm after excitation with light at different wavelength. The signals have been scaled so that they overlap at longer delay times. The higher the excitation energy, the smaller the GSB increase.

Such a behavior may suggest the presence of a energy barrier in the S_1 state for a process that brings additional molecules from the ground state to the excited state, increasing thus the bleach. This can happen only if an excited molecule runs into a ground state molecule, which involves a diffusion controlled process. But this cannot be the case, since at 1mM the theoretical molecular collision rate constant is on the order of hundreds of ns. The conclusion is that the molecules must be already close to one another at the moment of the photo-induced excitation, but not as a conventional ground state dimer, since there has to be the possibility to excite independently the two monomers in order to observe an increase of the GSB. We could then imagine that a significant fraction of pyrene molecules form a loosely bound dimer, possibly preassociated due to solvophobic interaction.

Such an interpretation would then contrast with Birks' theory of excimer formation, since it implies that the PIA at delay values bigger than 30 ps is already the absorption spectrum of pyrene excited dimer, which is actually expected to appear hundreds of ns after the excitation in Birks' model. In order to understand if the existence of loosely preassociated dimers and the conventional theory of pyrene fluorescence can coexist, we investigated the transient absorption of pyrene on the ns time scale and the time resolved fluorescence, whose results are presented in the next sections.

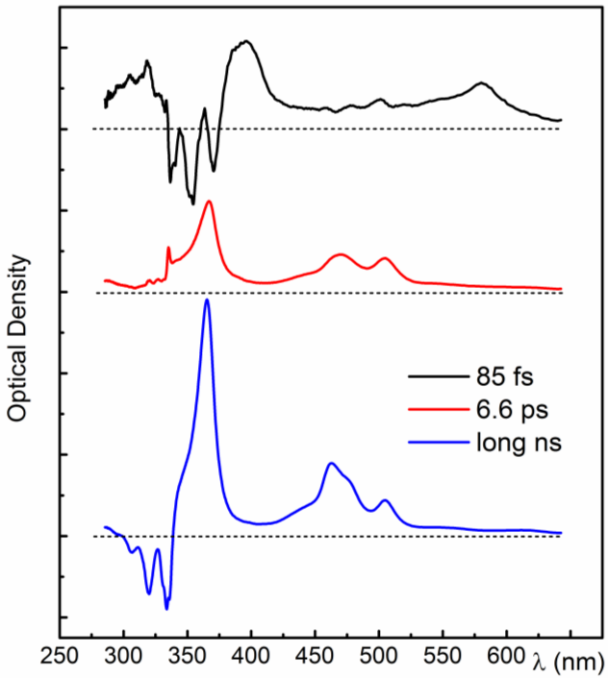

Fig 3.13 Species associated spectra obtained assuming a three-step rate model with the constants from the global fit: (85 ± 20) fs, (6.6 ± 0.5) ps and (5 ± 2) ns.

Fig 3.13 shows the SAS decomposition (see sec. 2.2.2) obtained from the global fits DADS. They represent the absorption spectra of the species involved in the dynamics, assuming a three-state rate model. In particular, we note that the spectrum of the S_2 state (black line) clearly shows a stimulated emission component (i.e. fluorescence from the S_2 state), which represents the mirror image of steady-state pyrene absorption spectrum.

3.5 Long time dynamics

In order to investigate the dynamics of the S_1 state and of pyrene excimer, the setup described

in sec. 2.2.4 for ns pump-probe experiment has been employed. The result for a 1 mM solution of pyrene in methanol excited at 334 nm is shown in Fig 3.14.

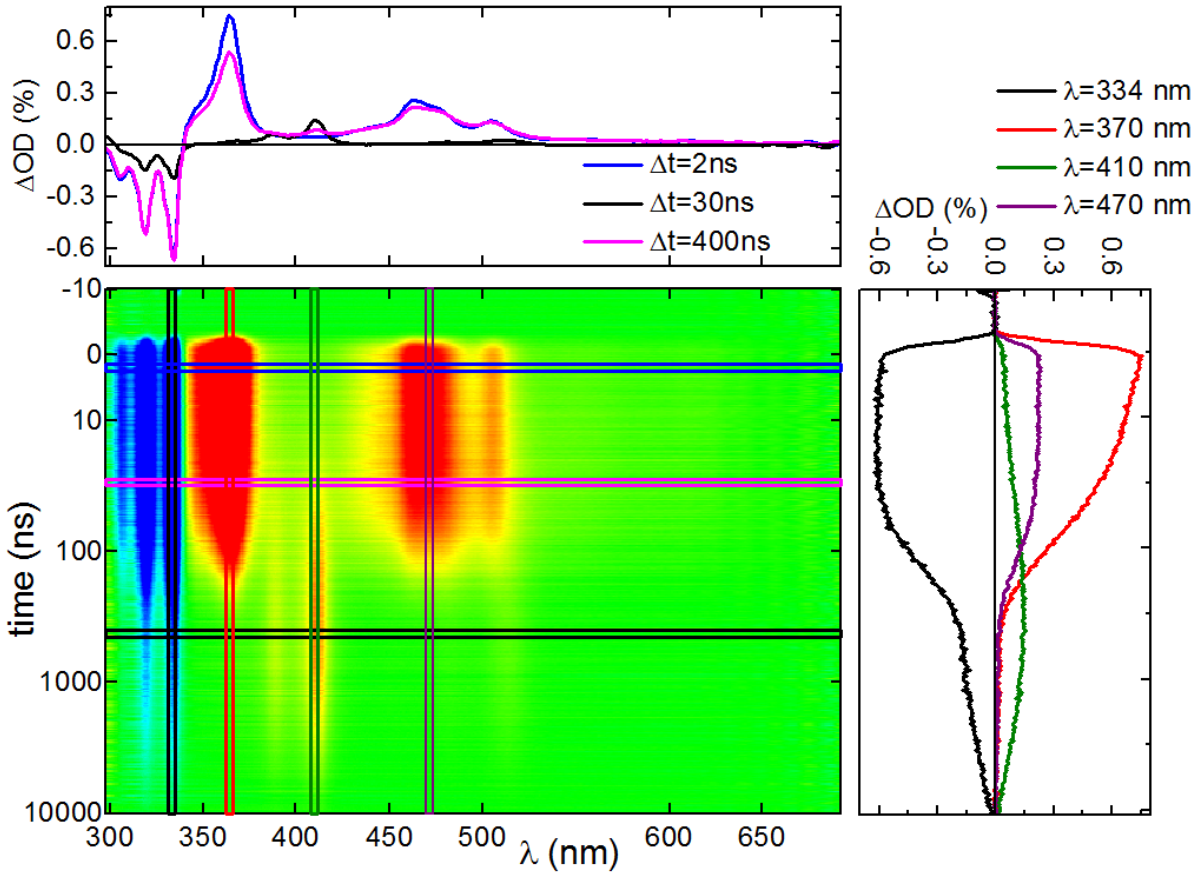

Fig 3.14 TA spectrum and profiles of 1mM pyrene in methanol after excitation at 334 nm.

The spectrum shows clear signature of the GSB below 340 nm and of the PIA between 340 and 550 nm, as well as of absorption from pyrene excited triplet state around 400 nm. The intersystem crossing from the S_1 singlet state to the triplet state of pyrene has been widely reported in the literature [Boh90]. In our case, we see the triplet signature increasing as the absorption from the S_1 decays and vanishing then with a longer time constant. Since the dynamics of aromatic molecules is affected (on the ns time scale) by quenching by the oxygen dissolved in solution [Par61, Bir70], the TA data in Fig 3.14 were collected in oxygen-free conditions, which have been obtained by pumping the solution with nitrogen before the measurement and by integrating a degassing apparatus (KNAUER Online Degasser) in the circuit of the flow cell. The solution has been degassed for at least two hours before the start of the measurement and during the measurement itself. An analysis of the time constants involved in the dynamics and of their behavior in relation with oxygen presence is given by

the DADS obtained from the global fit and displayed in Fig 3.15.

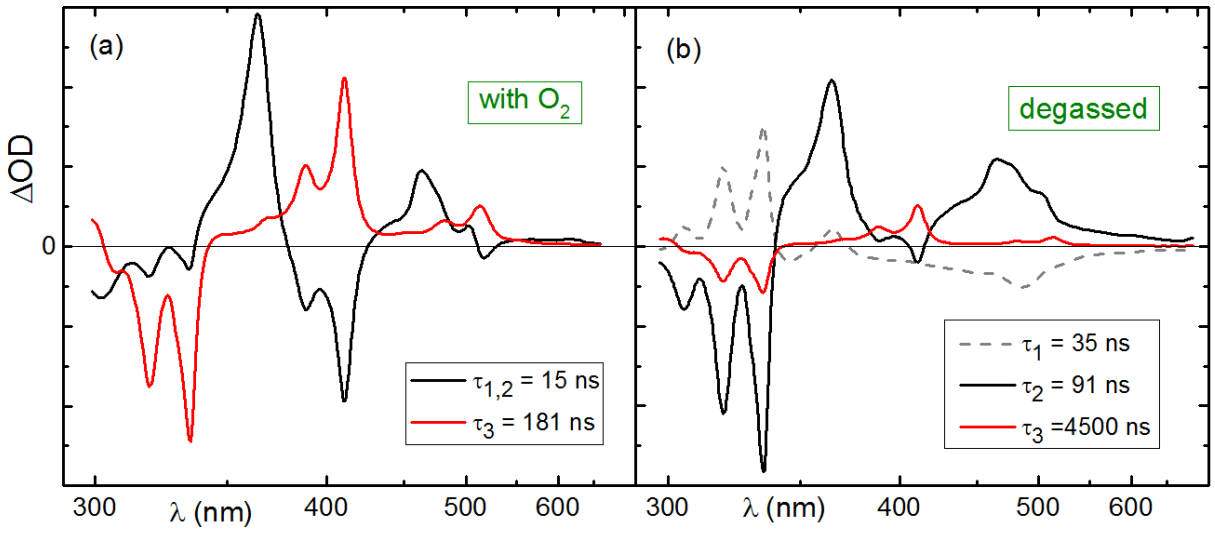

Fig 3.15 DADS obtained from a global fit analysis of the TA of a 1 mM solution of pyrene in methanol excited at 334 nm in presence (a) and in absence (b) of oxygen in solution.

Fig 3.15a and Fig 3.15b show the DADS for the TA of a non-degassed solution and of a degassed solution respectively. A first significant difference is that in the first case two temporal components could be resolved, whereas in the second case a third, shorter, time constant was needed in order to fit the data. The presence of oxygen in solution adds a decay channel, shortening thus the lifetime of the molecular states. The additional decay process is however dependent on the nature of the state involved and the decrease in the lifetime is then different for each state. We imagined that the shortest time constant in presence of oxygen $\tau_{1,2}$ = (15 ± 3) ns , which relates to the decay of S_1 and to the rising of the triplet signal, is actually a superposition of the two contribution of τ_1 = (35 ± 5) ns and τ_2 ~ (91 ± 10) ns in the oxygen-free case. The longest time constant τ_3 (which is (180 ± 30) ns with oxygen, and (4.5 ± 0.5) μs without oxygen) can be assigned to the decay of the pyrene triplet state.

No qualitative differences have been found when changing the excitation wavelength or the solvent. As an example in Fig 3.16 we show the transient spectra at different delays for a 1 mM degassed solution of pyrene in cyclohexane after excitation at 334 nm, where the rise of the triplet as the absorption from S_1 decays is clear to see. The absorption spectra of the triplet, pyrene cation and pyrene anion excited states taken from literature [Gre73] are reported too. We note how the triplet spectrum perfectly matches with the TA traces as well

as the fact that the cation and anion spectra occupy the same region as the visible wing around 470 nm of the absorption spectrum previously assigned to S_1.

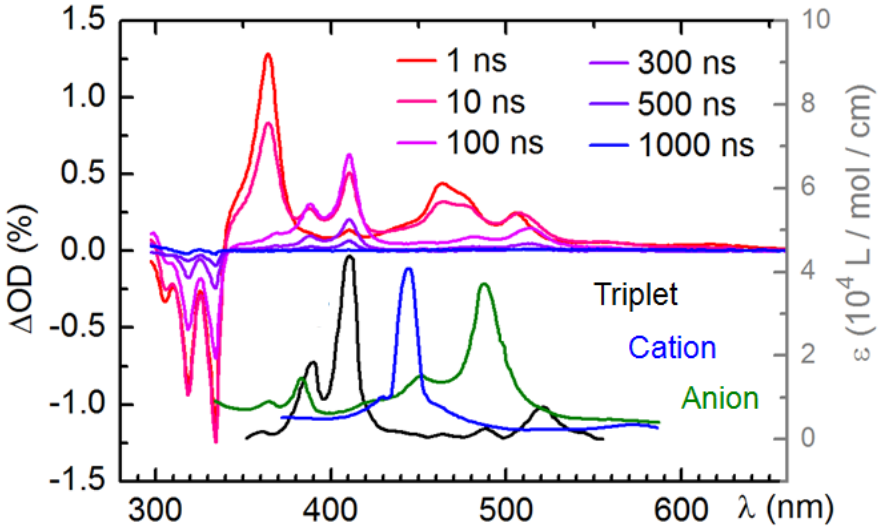

Fig 3.16 TA of 1mM pyrene in cyclohexane after excitation at 334 nm at different delay times. Absorption spectra of the triplet state [Hei69], pyrene cation and pyrene anion [Aal59] from literature are reported.

3.6 Fluorescence measurements

Time resolved fluorescence of pyrene in methanol and cyclohexane has been investigated with the setup described in sec. 2.3.2. Like in the pump-probe experiment, a degasser has been used in order to remove oxygen from the sample solution.

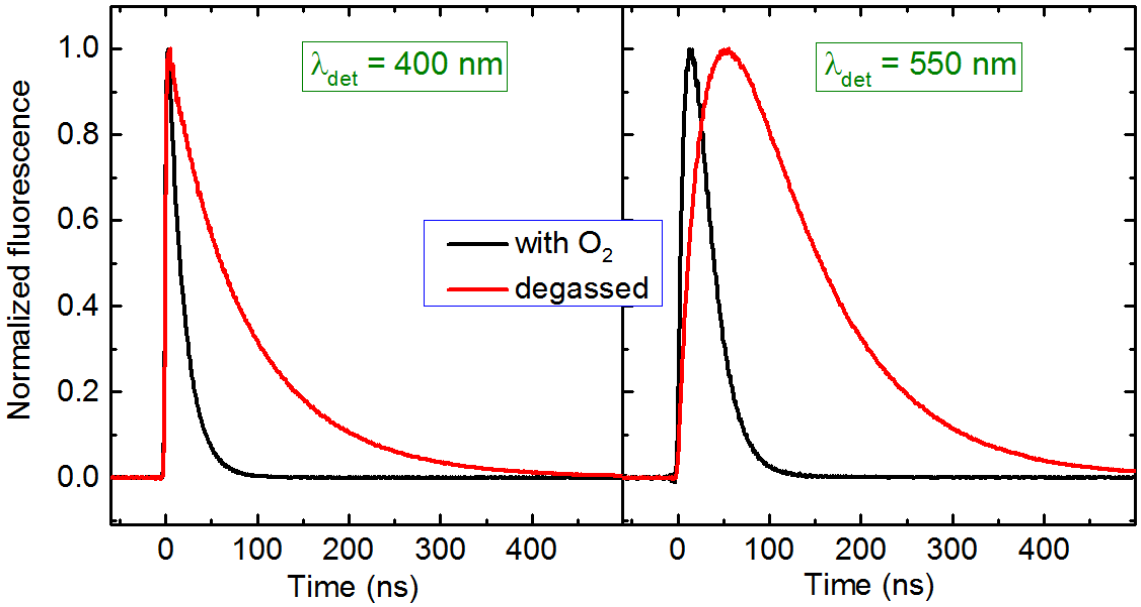

Fig 3.17 Comparison between the monomer (left) and excimer (right) time-resolved fluorescence of pyrene in methanol (1 mM) after excitation at 334 nm, in presence and in absence of oxygen.

Fig 3.17 shows the time behavior of the fluorescence emission of pyrene monomer (λ_{det} = 400 nm) and pyrene excimer (λ_{det} = 550 nm) after excitation into the S_2 state in methanol. Monomer fluorescence decays exponentially with a time constant of (90 ± 6) ns ($k \sim 1.11\times10^7\, s^{-1}$), in agreement with τ_2 found in pump-probe measurements, whereas the excimer signal rises with (35 ± 3) ns ($k \sim 2.86\times10^7\, s^{-1}$), corresponding to τ_1, and decays like the monomer with τ_2 ~ 90 ns. As expected, τ_2 results concentration dependent (τ_2 ~ 250 ns at 0.1 mM), whereas no significant variation has been found for τ_1.

Since Hanlon and Milosavljevic [Han13] reported a dependence of fluorescence on the excitation wavelength, we recorded fluorescence emission of pyrene in methanol and in cyclohexane after excitation to the lowest singlet excited state S_1 at 372 nm (see Fig. 3.18). The intensity of the pump light had to be increased in order to have a good signal, due to the very low absorption.

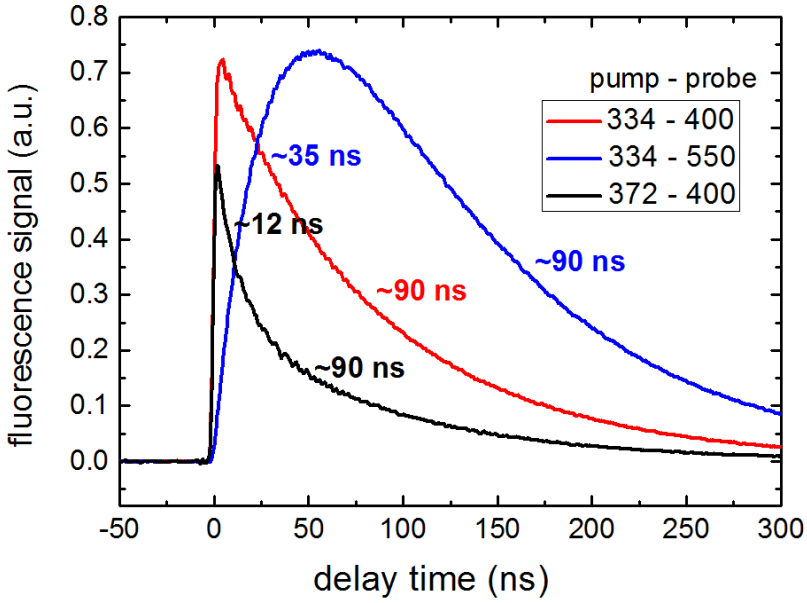

Fig 3.18 Fluorescence of 1mM pyrene solution in methanol. The red and the blue curves represent the signal from the monomer and the excimer respectively, after excitation to the S_2 state. The monomer fluorescence after excitation at 372 nm (black curve) shows a double exponential decay.

The signal from the excimer repeats the same trend as after excitation at 334 nm, whereas the monomer fluorescence could not be fitted with a single exponential decay. The decay is bi-exponential, with a fast component of (12 ± 3) ns beside the usual $\tau_2 \sim 90$ ns.

In order to investigate this unexpected result, we performed a more detailed scan of the excitation wavelength throughout the range of the S_1 state and fitted a double exponential decay to the monomer fluorescence. Fig 3.19 shows the results of the fits. The amplitude of τ_2 follows the trend of pyrene steady-state absorption spectrum. The fast component is present over all the explored range below the S_2 threshold, but its relative contribution becomes predominant around 369 nm excitation wavelength.

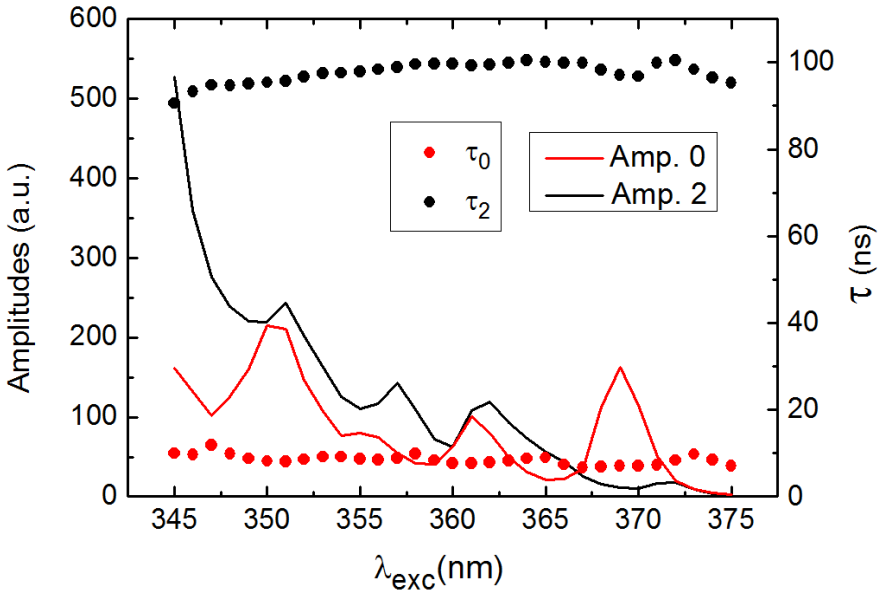

Fig 3.19 Fit results for the monomer fluorescence (λ_{det} = 380 nm) of 1mM pyrene in methanol after different excitations.

Fig 3.20 shows a comparison between the absorption spectrum and excitation spectra at different detection wavelengths. As can be seen, contrary to the 500 and 550 nm spectra the excitation spectrum at λ_{det} = 390 nm clearly deviates from the absorption spectrum at λ_{exc} = 369 nm, which are exactly the "spectral coordinates" where the fast decay component becomes predominant. This can be the signature of the presence of a very small amount of a second species in the sample, which is too little to be seen in absorption and can only be detected in the fluorescence emission. This additional impurity could be either some dirt in the sample or a photoproduct of the excitation of pyrene.

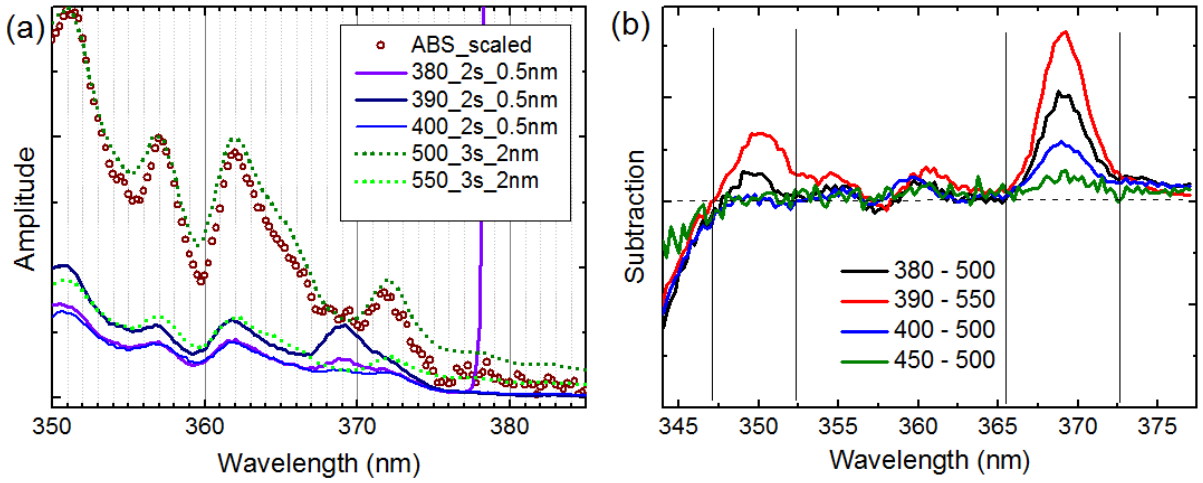

Fig 3.20 (a) Comparison between the steady state absorption spectrum of pyrene (scaled)

and excitation spectra at different detection wavelength. (b) Subtraction of excitation spectrum at 500 nm from excitation spectra at shorter wavelength show a significant deviation at λ_{exc} = 369 nm for the spectra around λ_{det} = 390 nm.

This additional species is present also in highly purified pyrene samples, so the involvement of a photoproduct seems feasible. Reports in literature of photo-degradation of pyrene in dichloromethane and acetonitrile have been found in ref. [Shi07]. In that case the derivatives have been assigned to 4,5,9,10-tetrahydro-pyrene.

We also performed irradiation experiments of pyrene in dichloromethane and methanol and found evidence of photo-degradation, more severe in dichloromethane than in methanol. In Fig 3.21 we show how heavily the absorption spectrum changed after being irradiated with a laser beam with similar features as in the time-resolved fluorescence experiment.

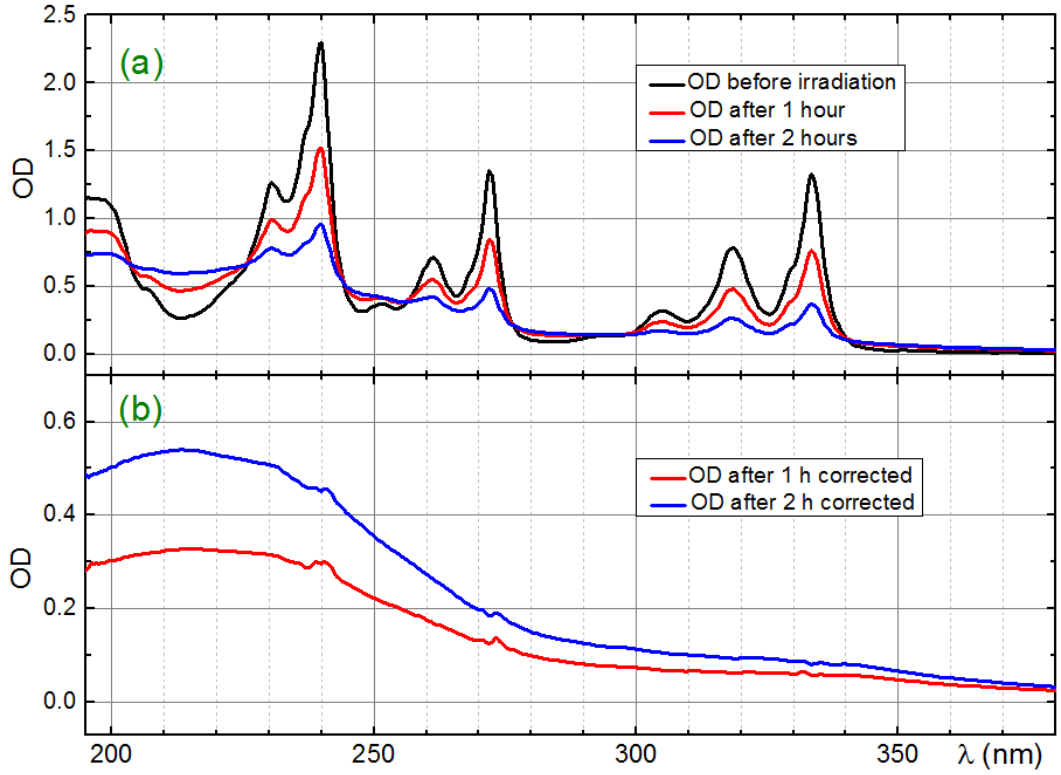

Fig 3.21 (a) Changes in the absorption spectrum of a 0.2 mM solution of pyrene in methanol in a 1 mm cuvette due to irradiation of the sample with 334 nm laser light. The laser delivered ~ 3 ns long pulses at a frequency υ = 1 kHz, with an energy E = 10 μJ. (b) Absorption spectra of the irradiated solution after subtraction by the spectrum of the non-irradiated pyrene solution. They represent the absorption spectrum of the photoproduct.

3.8 Discussion

In this chapter we reviewed some of the most relevant studies in literature about pyrene photodynamics and presented our experimental results. Birks developed a model to interpret pyrene fluorescence emission in terms of a collisions driven excimer formation process. According to the model pyrene exists in solution as monomer and after photoexcitation it can from an excimer if colliding with another monomer. Many successful improvements have been made to the model in order to fit the time-resolved fluorescence data and their concentration dependence. Recently Hanlon and Milosavljevic proposed a simplified version which works for dynamics after excitation to the S_1 state. Some values for the two time constants predicted by the model at 1mM are listed below:

[Bir63]:	$\tau_1 \sim 40$ ns;	$\tau_2 \sim 150$ ns	pyrene in cyclohexane
[Han13]:	$\tau_1 = (36.0 \pm 0.3)$ ns;	$\tau_2 = (182 \pm 2)$ ns	pyrene in decane

We performed time-resolved fluorescence measurements and we could fit the data with a monoexponential decay (τ_2) for the monomer and two exponentials for the excimer (τ_1 rise, τ_2 decay), with values at 1mM:

$\tau_1 = (35 \pm 3)$ ns;	$\tau_2 = (90 \pm 6)$ ns	pyrene in methanol
$\tau_1 = (37 \pm 6)$ ns;	$\tau_2 = (85 \pm 10)$ ns	pyrene in cyclohexane

As can be seen τ_2 in cyclohexane does not correspond to the value reported by Birks. Moreover, the trend of the decay times that we estimated is not always coherent with expectation, i.e. $\tau_2 \sim$ does not always increase as the concentration diminishes. For these two reasons we suspect the degassing procedure may have not been correct: oxygen might have diffused into the solution through the tubes of the circuit and a stationary equilibrium with the degassing might have taken place, which was however each time different.

Pump-probe experiments with a time resolution of ~ 75 fs were performed and revealed an ultrafast spectral signature of the absorption from the S_2 state, namely a band at 580nm, already reported in literature, and one at 400 nm together with a clear signature of the stimulated emission from S_2 state. The ultrabroad continuum light allowed us to probe transient absorption also in the near UV and thus to monitor the GSB recovery, no trace of which has been found in the literature. Vibrational relaxation in the S_1 state seems to happen in ~ 6.6 ps and the same time constant characterizes, according to the global analysis, an increase in the ground-state bleach. This relaxation process happens to be temporally and

quantitatively dependent on the excitation wavelength. An analysis of the characteristics of the process is given by the results of the single channel fit displayed in Table 3.2.

λ_{exc}	τ GSB @ 334 nm	Amplitude (vs ns)	τ abs @ 362 nm	Amplitude (vs ns)	τ abs @ 470 nm	Amplitude (vs ns)
334	(6.0 ± 0.5) ps	-0.6	(8 ± 1) ps	-0.6	(6.5 ± 0.5) ps	- 0.4
318	(7.2 ± 0.5) ps	-0.4	(11 ± 1) ps	-0.4	(6.7 ± 0.5) ps	- 0.3
305	--	--	(17 ± 2) ps	-0.3	(8 ± 0.7) ps	- 0.2

Table 3.2 Results of the single channel fit for the relaxation dynamics at three different detection wavelength. Time constant and amplitude of the component with respect to the amplitude of the long time decay are reported. As we can see, the magnitude of the relaxation gets smaller as the excitation wavelength is increased.

The relationship between the GSB increase and the relaxation of the absorption bands remains unclear. No further dynamics has been detected on the ps time scale.

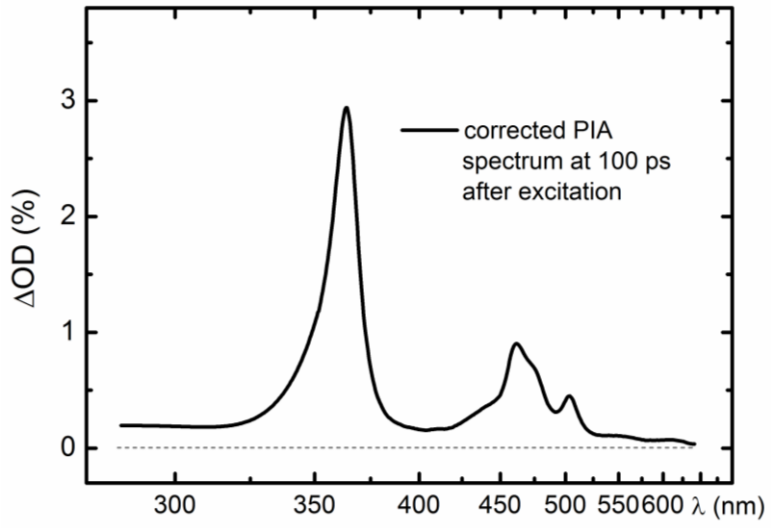

Fig 3.22 Photo induced absorption of S_1, obtained from the TA signal 100 ps after excitation and corrected for the GSB through subtraction of the steady-state absorption spectrum.

On the ns time scale we could detect the time constants τ_1 and τ_2 with similar values as in the fluorescence experiment, again with some discrepancies probably due to the oxygen presence. τ_1 fits a rise of the signal in the blue region of the spectrum, whereas the DADS related to τ_2 resembles, but not totally equals, the PIA of the S_1 state from the ps measurements,

overlapped with the rising spectrum of the triplet state. A decay constant for the triplet τ_3 ~ 4500 ns (Fig 3.15) has been determined for 1mM pyrene in methanol.

The wavefunction describing pyrene excimer is a configuration interaction of exciton states and charge transfer states. Indeed, the excimer absorption spectrum is in the region of the pyrene cation and anion absorptions (Fig 3.16), but also part of the monomer absorption is present there.

The GSB increase that we detected carries the binding consequence that a fraction of the molecules is excited picoseconds after the interaction of the pump pulse with the sample. To explain this feature, we propose another model for pyrene photodynamics (see Fig 3.23), starting with the hypothesis of loosely preassociated dimer bound by solvophobic interaction, which absorbs like a monomer and after ~ 7 ps shares the excitation with the other monomer.

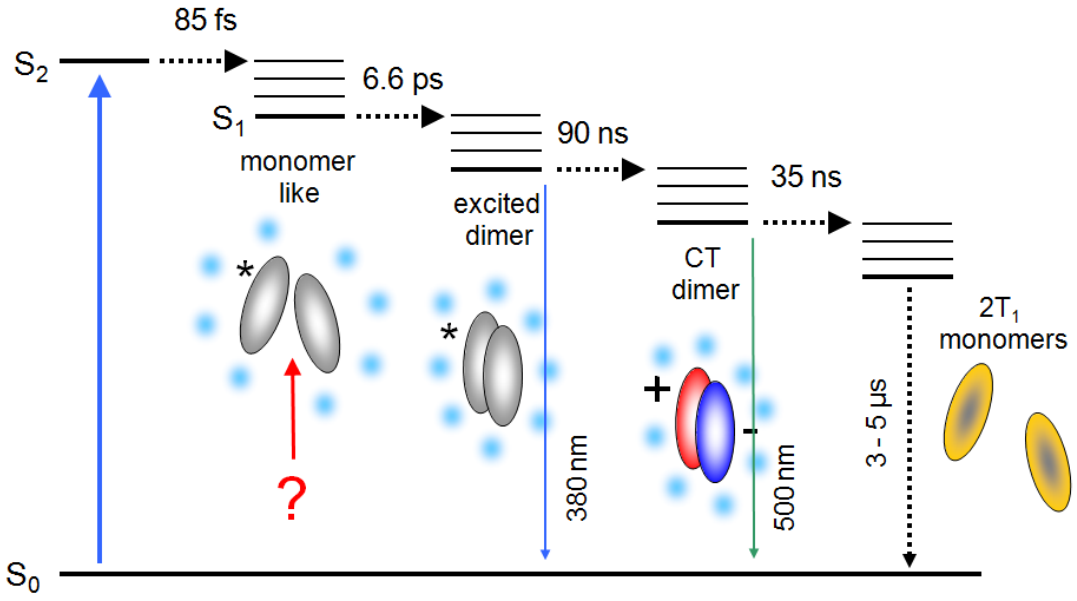

Fig 3.23 Proposed model for pyrene photodynamics. Pyrene exists in solution as a weakly preassociated dimer, i.e. solvophobic interactions bind two monomers in a solvent cage but without them forming a ground state dimer. The monomers can be separately excited to the S_2 state and, after the ultrafast conversion to S_1 state, the excitation is shared within ~ 7 ps with the other monomer in the solvent cage, forming thus the excimer. The excimer fluoresces in the near UV and after a collision with another pyrene molecule can decay into a charge-transfer state, which in turn fluoresces in the blue and decays into two triplet monomers.

The PIA in Fig. 3.22 would then be the absorption spectrum of the excited dimer. In order to

explain the concentration dependence of the decay of this species, we suppose a collisions (with other pyrene molecules) driven decay of the excimer into a charge-transfer dimer, which in turn decays into two monomers in the triplet state. The involvement of a charge-transfer state has been presumed because of the previously mentioned overlap of the spectra of pyrene ions and the DADS from our experiment.

Such a model based on preassociation could work only if we assume that pyrene molecules exist in solution only as loosely bound molecules, which is not in agreement with literature [And92]. It is likely then that this preassociated dimer does not correspond to the ground-state dimer of literature.

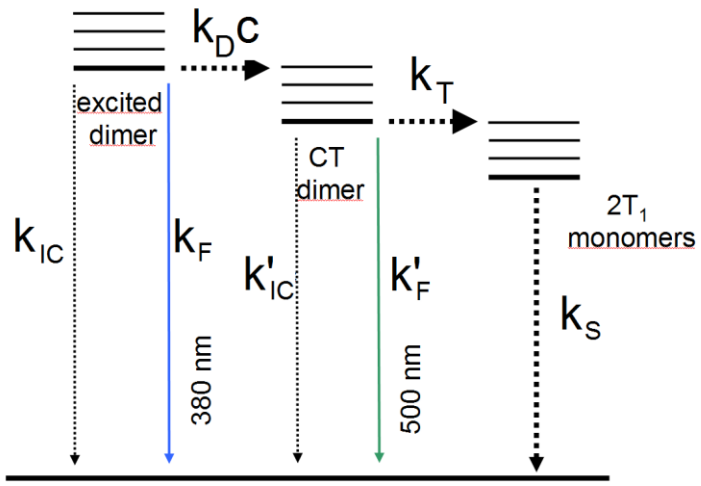

Fig 3.24 Definition of the involved rate constants, where IC means internal conversion and F fluorescence. As the excimer decay into a CT state is collisions driven, the relative rate constant $k_D c$ is proportional to pyrene concentration. We define also $k_E \cong k_F + + k_{IC} + k_D c$ and $k_{CT} \cong k'_F + k'_{IC} + k_T$.

From a mathematical point of view this model is identical to the one of Birks (in the Milosavljevic's version) but with the excimer in place of the monomer and the charge-transfer dimer in place of the excimer. The fluorescence emission is then correctly predicted. In Fig 3.24 the rate constants that we used are introduced. Equations give a linear dependence on concentration of the ratio between charge-transfer dimer fluorescence in the blue and the excimer fluorescence:

$$\frac{I_{CT}}{I_E} = \frac{k'_F}{k_F}\frac{k_D}{k_{CT}}c$$

where I represents the fluorescence quantum intensity integrated in time all over the emission duration [Bir63].

The solution of the rate equations gives the following time behavior for the populations of the involved states, i.e. the excimer (E), charge-transfer (CT) and triplet state (T):

$$\begin{cases} [E] = e^{-k_E t} \\ [CT] = \dfrac{k_D c}{k_{CT} - k_E}\left(e^{-k_E t} - e^{-k_{CT} t}\right) \\ [T] \propto e^{-k_S t} - \dfrac{k_{CT} - k_S}{k_{CT} - k_E} e^{-k_E t} + \dfrac{k_E - k_S}{k_{CT} - k_E} e^{-k_{CT} t} \end{cases}$$

where the concentrations have been normalized to the initial value of the excimer concentration. As we see, the excimer undergoes a monoexponential decay with $k_E = 1/\tau_2$, the population of the charge-transfer state rises with $k_{CT} = 1/\tau_1$ and decays with k_E. The triplet trend is affected by all the three time components τ_1, τ_2, and $\tau_3 = 1/k_S \sim 4500$ ns. Clear trace of the triplet absorption spectrum has been found in the τ_2 and τ_3 DADS, but no striking evidence of it in the τ_1 DADS could be detected. We must say, however, that the role of the triplet state in this model could be oversimplified: a decay channel to the triplet could be possible also for the excimer and the possibility of reversible decays should be considered. Further experimental investigations would then provide more insight into these aspects.

4. Indole photodynamics and generation of solvated electrons

4.1 Introduction

Indole is an aromatic heterocyclic molecule, composed by a benzene ring fused to a five-membered nitrogen containing pyrrole ring. It is the chromophore of tryptophan, which is one of the 20 essential human amino acids, with a strong absorption in the near UV region of the sun light spectrum. Indole and tryptophan fluorescence has been extensively exploited as a probe in a huge variety of studies involving protein dynamics [Sza80, Bee85, Che98, Sch05, Zha06, Lak06], thanks to its high sensitivity to the molecular environment [Lak06]. Further interest in these molecules comes from the fact that they exhibit single photon ionization [Ben74] as an additional decay channel, which is connected, in the condensed phase, with the generation of solvated electrons. These reasons motivated numerous theoretical and experimental studies.

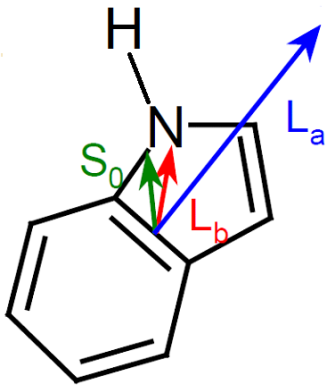

Fig 4.1 Molecular structure of indole and permanent dipole moments computed from ab initio methods for the ground state S_0 and the lowest excited singlet states, taken from ref. [Biz04].

Indole lowest singlet excited states have ππ* character and are identified following Platt's nomenclature [Pla49] as ^1L_b (S_1) and ^1L_a (S_2). These states are responsible for fluorescence emission and for the first absorption band. The absorption spectrum between 300 and 240 nm

consists in the superposition of a broad unstructured band from the ^1L_a state and a weakly structured band attributed to the ^1L_b state. The level of sharpness of the structure depends on the solvent as it is more pronounced in non-polar solvents. Dependent on the solvent polarity are also the Stokes shift and the spectral shape of the fluorescence emission, as one can see in Fig 4.2, and the fluorescence quantum yield [Kle81].

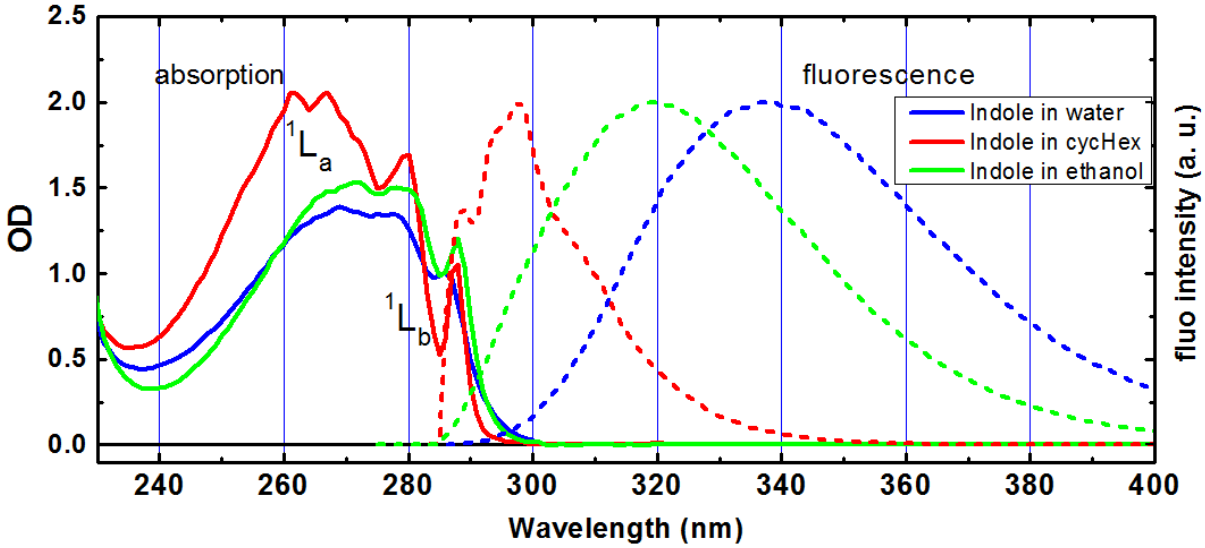

Fig 4.2 Steady-state spectra of indole in non-polar (cyclohexane) and polar (ethanol and water) solvents.

A gradual spectral redshift of fluorescence was detected by adding increasing fractions of ethanol in a cyclohexane solution of indole, and this was ascribed to hydrogen bonding of the hydroxyl group of ethanol to the imino nitrogen of the indole ring as well as to usual dipole-dipole interactions between indole and the solvent molecules [Gri88, Lak06]. The same phenomenon, however, has also been interpreted as a consequence of the formation of exciples, formed by excited indole and polar solvent molecules [Wal67].

Indole exhibits also quite a complicated decay dynamics, which besides fluorescence involves also temperature dependent processes, like photoionization, and intersystem crossing to the triplet state, which does not depend on temperature [Kle81].

Several studies on the isolated indole molecule locate the origin of the ^1L_b state at about 35 233 cm^{-1} (284 nm) and that of the ^1L_a state about 1000 - 1500 cm^{-1} over ^1L_b [Mon12]. Nowadays, the general accepted explanation for the dependence of fluorescence on the solvent polarity involves a state reversal mechanism driven by solvation effects [Lam86]. This means that, since the permanent dipole moment of the ^1L_a state is much bigger and has a

different orientation than that of the ground state and of ^1L_b state (see Fig 4.1), the interaction of the excited molecule with the polar solvent molecules lowers the energy of the ^1L_a more than that of the ^1L_b. A strong vibronic coupling between the two excited states permits internal conversion from one to the other, so, regardless of which of them has been excited, the fluorescent state is always the lower one, which happens to be the ^1L_b in gas phase and non-polar solvent and the ^1L_a in polar environment.

Recent studies stressed the importance of another excited singlet state, namely the S_3 state with $\pi\sigma^*$ character, which has very low absorption cross-section, but crosses the potential energy surface of the $\pi\pi^*$ states and presents a dissociative surface along the N-H bond [Sob02, Mon12]. Internal conversion from the ^1L_a state to the dark $\pi\sigma^*$ state is thought to be the key mechanism that can explain the indole ionization process and the generation of solvated electrons. Convincing experimental evidence to this argument is however still lacking [Lip04].

Despite indole and tryptophan photodynamics has been subject of several studies in the last fifty years, many loopholes remain. Very few time resolved experimental studies probing with a white light continuum are available [Hir89, Sai97, Peo99, Biz04, Sha10], despite the deep insight into molecular processes offered by this technique. For this reason we present in this chapter the results of the application of the pump-probe setup described in chapter 2 to the investigation of the indole photodynamics.

4.2 Previous results and ultrafast branching model

Starting point of our investigation is the PhD thesis of Tanja Bizjak [Biz04]. Bizjak performed transient absorption experiments by exciting indole at 270 nm and probing the delayed absorption with a Sapphire white light continuum limited to the visible range (from 460 nm to 720 nm). She studied solutions of indole in cyclohexane, ethanol and water, as well as neat water.

Indole transient absorption in cyclohexane and ethanol showed a broad ESA band, with a maximum at 640 nm, rising steeply, faster than the time resolution of the experiment (~ 80 fs). Subsequently, a rise and a decay of the signal with a time constant of about (6.5 ± 2) ps were detected in the case of ethanol and cyclohexane, respectively. The absence of a gradual spectral shift in the spectra was interpreted as a population transfer from ^1L_b to ^1L_a state in the

case of ethanol and vice versa in cyclohexane (as depicted in Fig 4.3), in agreement with steady-state fluorescence and employing the hypothesis of an ultrafast state reversal in polar solvents. The occurrence of the mentioned rise and decay is explained by a stronger ESA in the ^1L_a state, which gets populated in ethanol and depopulated in cyclohexane.

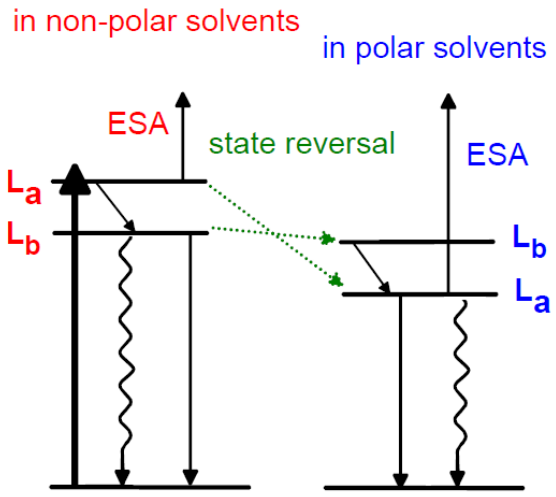

Fig 4.3 Model proposed by Bizjak in order to explain the correlation between steady-state spectra of indole in solvents with different polarity and the behaviour of indole molecular state with respect to solvation.

The possibility of photoionization of indole for excitation at 270 nm opens an additional relaxation channel in water. Bizjak's transient experiments revealed a broad maximum in the region between 620 and 700 nm, with the absorption rising within the time resolution and relaxing on a timescale of 350 fs. The interpretation of the spectrum turned out to be quite complex, due to the wide overlap of the absorption spectra of the numerous species contributing to the photodynamics: namely excited indole molecules, indole triplets, indole radical cations, neutral indolyl radicals and solvated electrons. Their spectra are shown in Fig 4.4. Experiments with 1-methylindole, which is unable to perform hydrogen transfer and yields though similar transient absorption dynamics as indole, proved that the solvated electron originates from electron transfer also in the case of indole and removed the indolyl radical from the involved species.

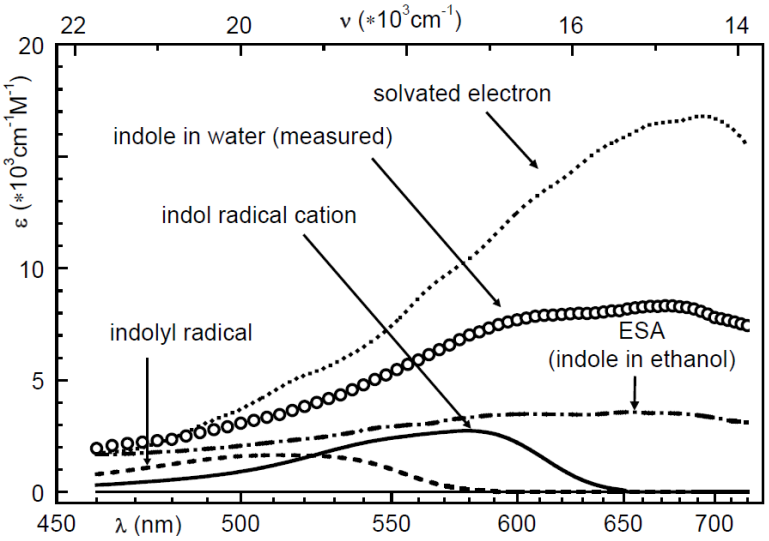

Fig 4.4 Absorption spectra of the different species that contribute to indole photodynamics in water, according to [Biz04]. The different spectra have been combined to fit the actual TA signal in water.

The species associated spectra have been fitted to the transient absorption of indole in water using the photoionization quantum yield ϕ_{ion} as parameter to be determined. The model developed by Bizjak (see Fig 4.5) suggests an immediate branching of the excited state to a charge transfer to solvent state (CTTS) and to a fluorescing state, which is the ^1L_a state due to the occurred state reversal. A fluorescence lifetime of (3.6 ± 1.0) ns was estimated from the radiative lifetime and the fluorescence quantum yield. The CTTS integrates an indole radical cation and a presolvated electron, which further relaxes to a fully solvated electron with a time constant of 350 fs and can then be excited from the ground s-like state to a p-state.

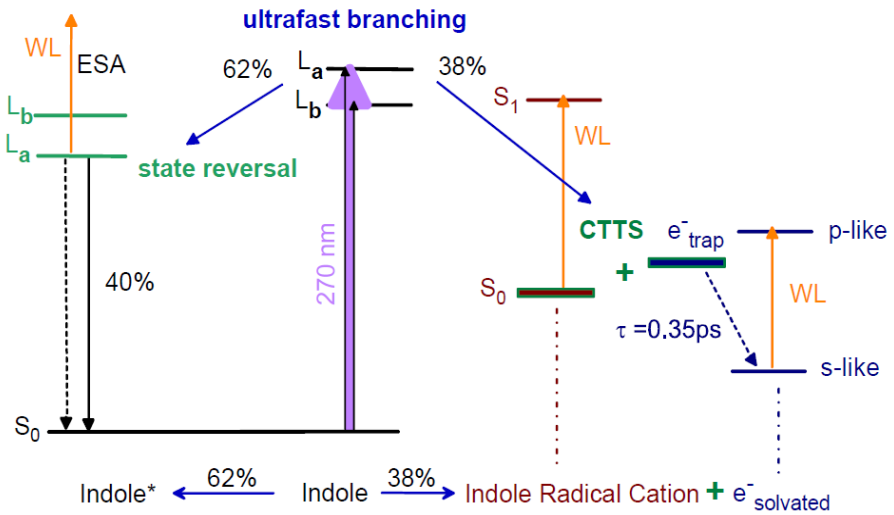

Fig 4.5 Schematic representation of the model developed by Bizjak [Biz04] to explain photodynamics of indole in water. An ultrafast branching occurs right after excitation: a fraction of the excited molecules undergo photoionization forming a radical cation and a CTTS state, the rest fluoresce from the ^1L_a state, the energy of which has lowered due to solvation. The fraction of ionized molecules was estimated through the result of the fit for the photoionization quantum yield: $\phi_{ion} = 0.38 \pm 0.10$.

4.3 Transient spectroscopy in jet: characterization of the setup

As already mentioned, time resolution in transient spectroscopy is limited not only by the length of the pulses, but also by the signal arising from the coherent interaction between pump and probe that takes place in the solution volume and in the glass windows of the sample holder. The magnitude of this signal, which masks the very first and fast photodynamics of the sample, can then be partially reduced by removing the sample holder as a whole. This goal has been achieved through the construction of a wire-guided thin liquid jet (see Fig 4.6). Another important reason to use a liquid jet instead of a flow cell is avoiding the deposition of photoproducts on the windows of the latter, which phenomenon happens to be significant in the case of indole [Peo99]. We actually performed pump-probe measurements with indole in a flow cell too, and the resulting spectrum was dominated by a strong fluorescence signal, constantly rising during the acquisition time coming, from the deposited photoproducts.

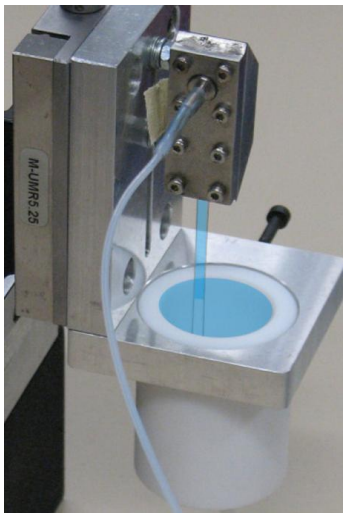

Fig 4.6 Picture of the realized setup for the production of a liquid jet.

The liquid jet has been built following the setup described in [Lai06,Tau03] but instead of using an upper reservoir from which the solution flows by gravity into the wired guide, we pumped the solution directly into the jet. The setup consists of two stainless steel plates clamping a 95 μm stainless steel wire, bent to form an inverted U, 3 mm wide. The solution is injected from a gear pump into the space delimited by the plates and the wire, building thus a thin film which leaves the housing flowing between the wired-guide sustained by surface tension and is collected by a reservoir from which it is then driven into the pumping circuit.

The thickness of the film can be easily regulated between 20 μm and 200 μm [Mai10] by varying the flow speed or the diameter of the wire or the width of the jet. We characterized the thickness profile of the jet by measuring the absorption of a 272 nm laser beam from a 15 mM solution of indole in water flowing in the setup and using then the Beer-Lambert law. The measured profile is shown in Fig 4.7.

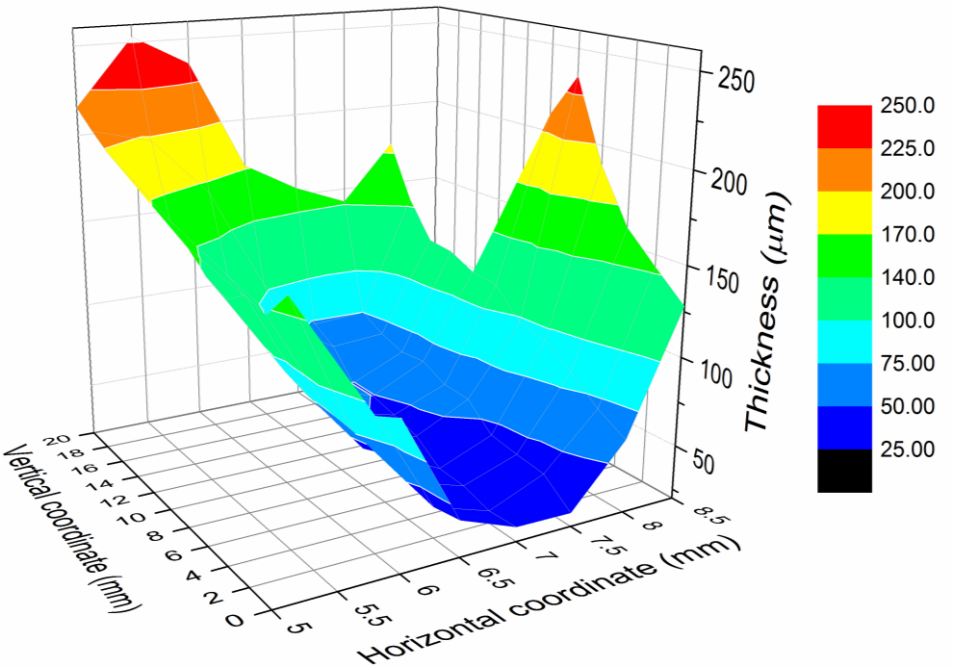

Fig 4.7 Measured thickness of the obtained liquid jet, as a function of an orthogonal set of axes spanning its surface.

In the lower and central part of the jet, the thickness of the film reached a thickness of about 30 μm on a region significantly bigger than the size of the probe beam. Similar conditions of the jet have been adopted for the pump-probe experiments on indole, with particular care for the stability of the flow and looking for the minimum distortion and refraction of the laser beams travelling through the film. The limited thickness of the liquid film required high

concentrated solutions in order to obtain a good signal, so in each of our experiments 15 mM solutions of indole have been used.

In order to determine the time resolution of the setup, a transient absorption spectrum of neat water in jet has been recorded. The signal consists in the bare coherent artifact resulting from the simultaneous nonlinear interactions of the pump and probe beams (see Fig 4.8). It has been fitted with a Gaussian function and its first two derivatives and the FWHM was found to be lower than 50 fs all over the spectrum where the artifact was detectable. The value of 50 fs has been subsequently taken as time resolution for the fits of the indole transient data.

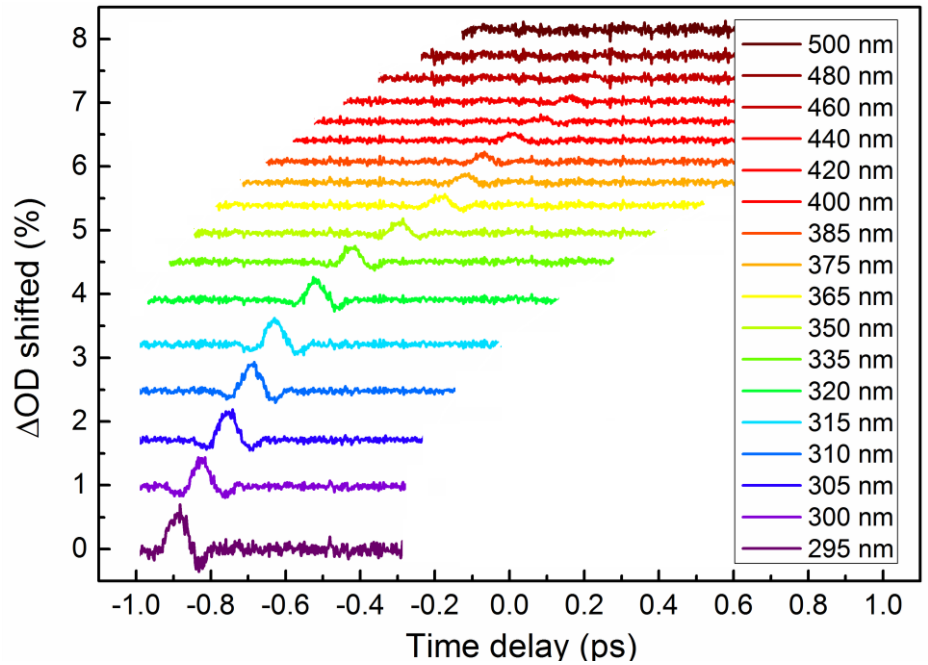

Fig 4.8 Stack graph of several time traces at different detection wavelengths of the TA of neat water flowing in our liquid jet setup. The signal shows, especially in the UV region, the shape of the coherent artifact, the width of which has been interpreted as the time resolution of the spectroscopy setup. Data courtesy of Roland Wilken.

A test of the reliability of the jet setup for transient spectroscopy has been made by comparing the signals obtained from a reference molecule in jet and in a cuvette. The molecule in question is a kind of flavin, an organic compound that had already been subject of thorough transient spectroscopy studies [Meg11]. As explained in sec. 2.2.1, the intensity of the TA signal is proportional to the absorption (i.e. the ratio, usually named A, between transmitted and incident intensity) of the pump beam, so we arranged the two experiments so that this

ratio would be comparable. We measured the spectra of a 3 mM solution of flavin in ethanol flowing in a ~ 30 μm thick liquid jet, and of a 1 mM solution contained in a 100 μm cuvette. The signal has been scaled in each case with the factor 1/A in order to properly compare the results, which are shown in Fig 4.9. As one can see, apart from a little discrepancy in the overall amplitude (which might be attributed to the difficulties in measuring with precision the pump beam absorption from the jet), the spectral signature of the transient data are actually very similar at all the time delays, thus confirming that pump-probe experiments in our jet setup yield reliable results.

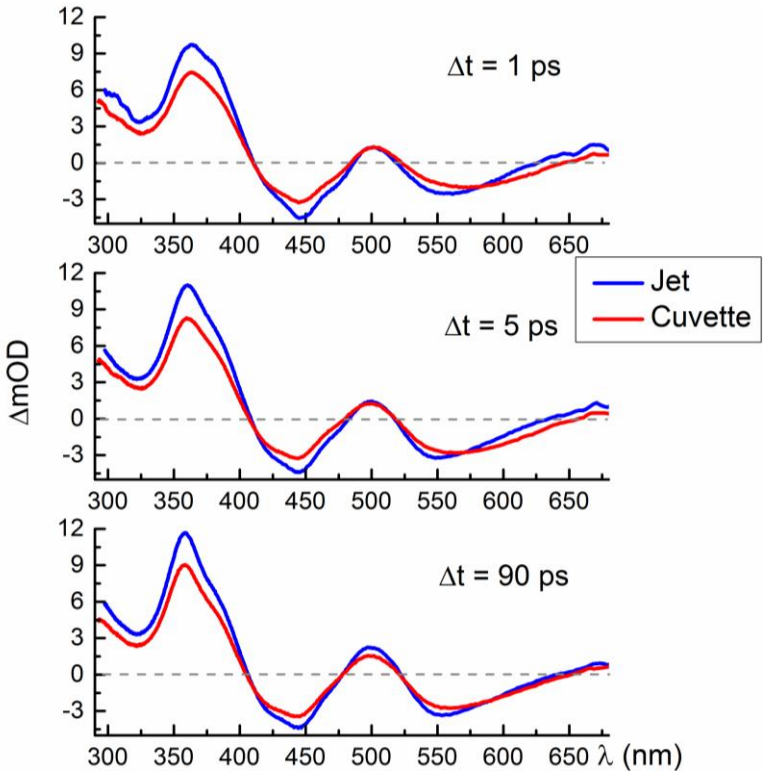

Fig 4.9 Comparison at different time delays of the TA of flavin in ethanol, measured in a flowing jet and in a cuvette. The two curves show significant agreement throughout the whole spectrum. The data have been scaled by the factor 1/A (A_{jet} = 0.43 and $A_{cuvette}$ = 0.51).

4.4 Pump-probe spectroscopy of indole in different solvents

4.4.1 Transient absorption in water

One of the purposes of our investigation of the indole dynamics is to understand from which excited state the photoionization and generation of the solvated electron take place. According to experimental studies on the isolated indole molecule [Mon12], the dark πσ* state with dissociative character can only be accessed after excitation above the ^1L_a state threshold at 273 nm. An excitation dependent photodynamics is then expected, at least with respect to the solvated electron component. For this reason we performed pump-probe experiments on a 15 mM solution of indole in water with pump pulses at different wavelengths (see Fig 4.10), particularly addressing the ^1L_b state, where we expect not to detect the dynamics induced by the photoionization.

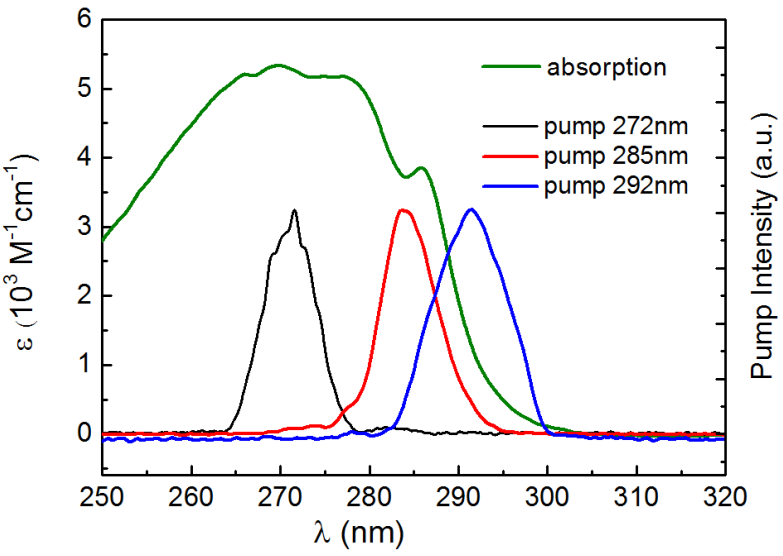

Fig 4.10 Spectra of the three different pump beams that have been used to excited indole solution.

Fig 4.11 shows the transient absorption spectrum of indole in water measured in a liquid jet with a resolution of 50 fs and excitation wavelength of 272 nm.

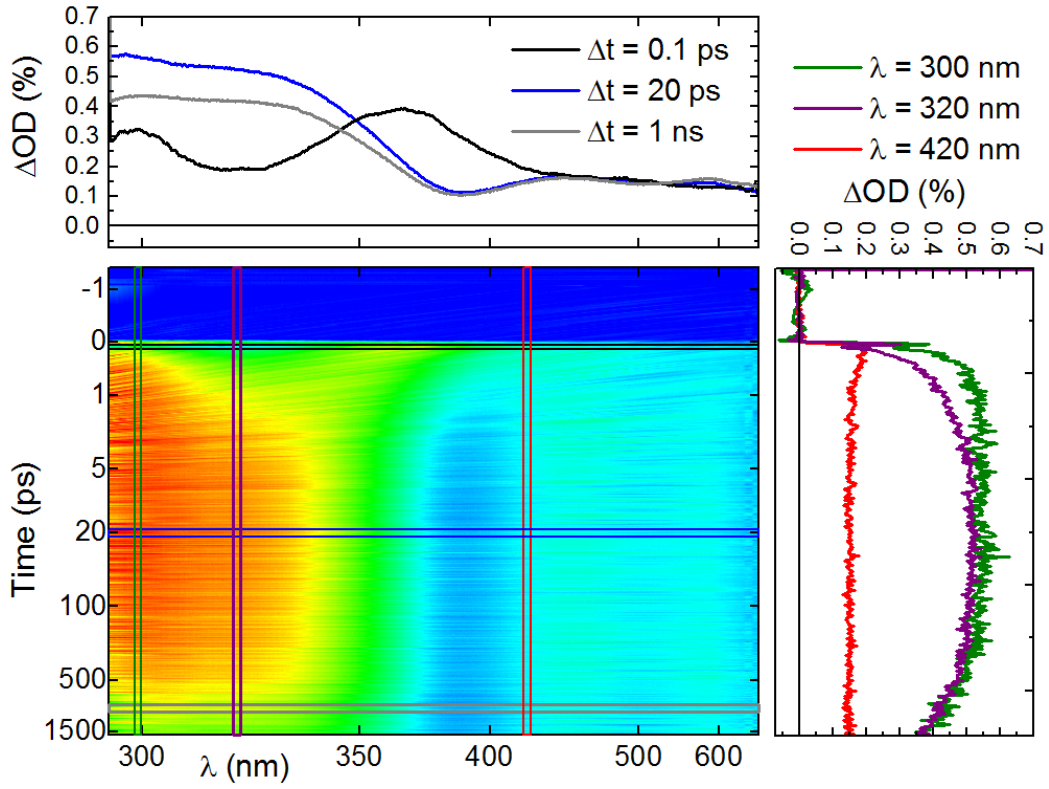

Fig 4.11 TA spectrum and profiles of indole in water (15mM) after excitation at 272 nm.

The spectrum consists mainly in a flat and weak absorption in the visible, rising within the time resolution and with no dynamics in the first 1.5 ns, and a broad absorption band in the near-UV region of our probe light. As already reported in preliminary studies by N. Krebs [Kre13], a band shift of the absorption in the UV is clearly visible: a band rises at ~ 365 nm within the time resolution and undergoes a blue shift of about 3500 cm^{-1}, which is completed after 3 ps.

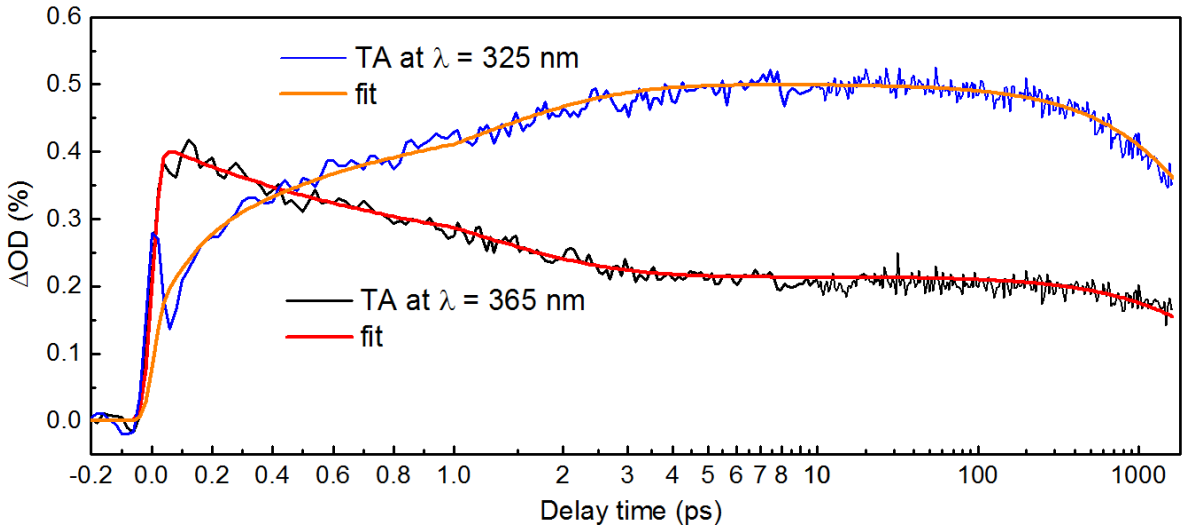

Fig 4.12 Time traces and relative fit of the TA of indole in water, at the starting and ending points of the shift of the absorption band.

However, unlike the results in [Kre13], an additional absorption band at 300 nm appears instantaneously and further grows with a time constant of (130 ± 30) fs, overlapping the shifting band. What actually catches the attention the most is the absence of the broad peak in the red region of the visible that characterizes the absorption of the solvated electron, widely reported in literature, both for indole and tryptophan and for neat water. Moreover, this band was clearly present also in the work of Bizjak, whose experiments were performed in a liquid jet too, only thicker than ours (Bizjak estimated a thickness of 120 μm). The absence of dynamics in the visible region on the ps time scale was confirmed also from the global fit, the DADS of which are displayed in Fig 4.13. A time constant of (1.1 ± 0.2) ps manifestly describes the band shift from 365 nm to 325 nm, and the absorption in the UV shows a decay with a (5 ± 2) ns time constant, which roughly matches the reported fluorescence lifetime of the indole excited state [Sai97, Sza80].The presence of a blue shift of the excited state absorption agrees with the hypothesis of a state reversal between the two lowest excited states of indole, that is the lowering of the energy of the states due to the interaction between the solvent molecules and the dipole moment of the excited indole.

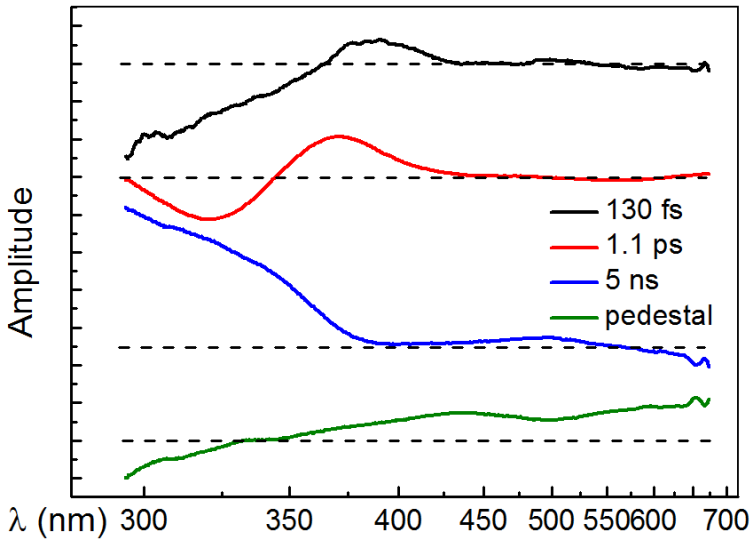

Fig 4.13 DADS calculated from the TA spectrum of indole in water.

Surprising is also the result of the comparison of the transient spectra of indole in water at different excitation wavelengths. Pump pulses centred at 372, 385 and 392 nm have been employed (see Fig 4.10), the last of which was meant to specifically excite the ^1L_b state and

not generate any solvated electron, the photoionization threshold in water being of 4.35 eV (~ 285 nm) [Gra79,Ber80]. As Fig 4.14 shows, no significant spectral difference between the three experiments can be observed at any time delay.

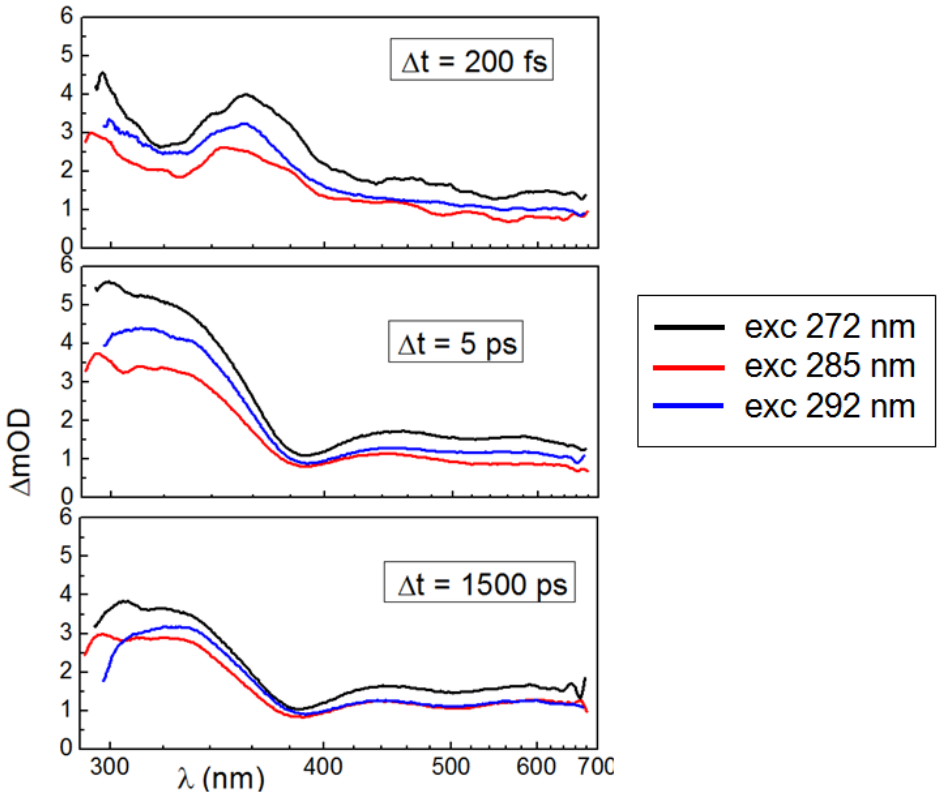

Fig 4.14 Comparison between the TA signal of indole in water after excitation at different wavelengths. No significant differences have been detected at any time delay.

4.4.2 Transient absorption in ethanol and cyclohexane

The ionization energy for indole in ethanol is reported to be 4.85 eV (~ 255 nm) [Ber80]. We performed pump-probe experiments with excitation light at 272 nm (see Fig 4.15), not expecting thus any signal from solvated electrons, nor from indole radicals.

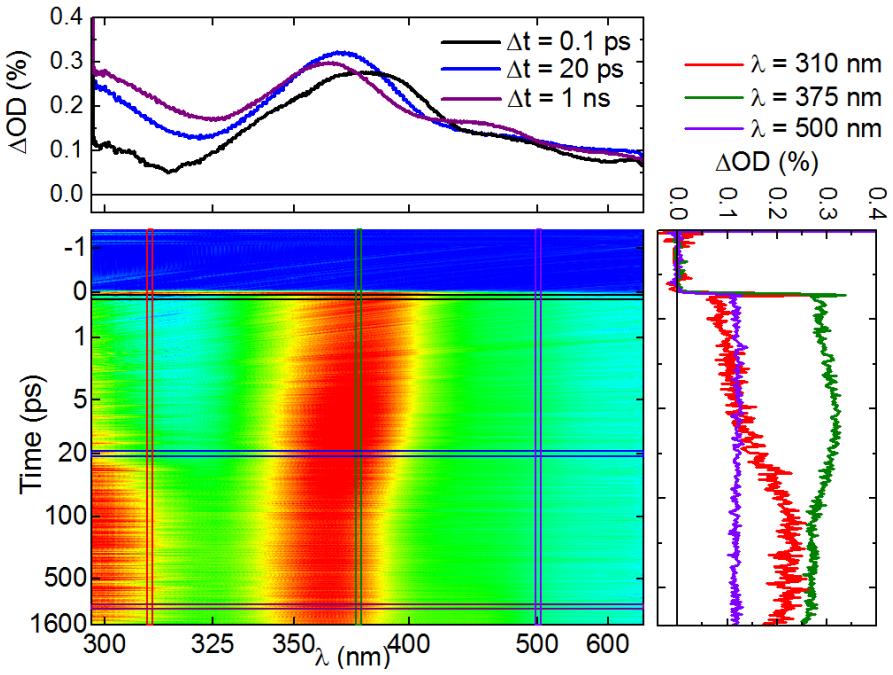

Fig 4.15 TA spectrum and profiles of indole in ethanol (15mM) after excitation at 272 nm.

The measured TA spectrum consists mainly of:

- a broad absorption band appearing around 377 nm within the time resolution and subsequently shifting by about 1000 cm^{-1} to the blue. The time evolution of the spectral position of the band maximum has been fitted, yielding two time constants: (4 ± 1) ps and (35 ± 4) ps. Analogous values resulted from the global fit analysis, confirming the reliability of this method (see Fig 4.16). This analysis suggests that the 4 ps component describes an increase of the signal that could be interpreted as a relaxation process.

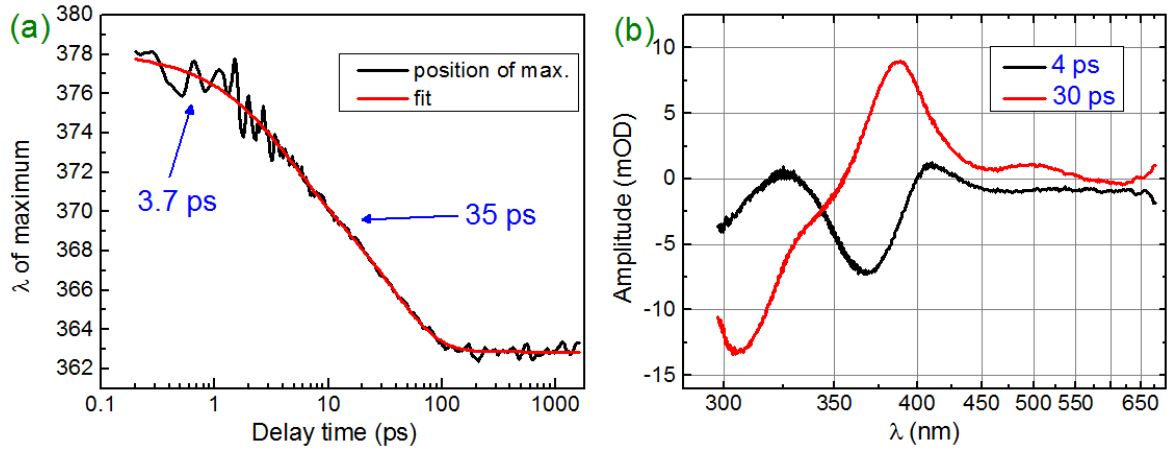

Fig 4.16 (a) Spectral position, and relative biexponential fit, of the maximum of the

shifting band as a function of the time delay, obtained by fitting a parabola to the absorption peak. (b) Short time DADS (the long time ones are shown in Fig 4.18) from the global fit of the TA spectrum.

- a second absorption band that appears at 300 nm in (30 ± 5) ps. The appearance of this band can be connected to the shift of the previously mentioned band at 377 nm. However, a comparison of the transient signal with the steady state fluorescence spectrum of indole in ethanol reveals a spectral correspondence between the latter and the dip in the absorption located between the two bands (see Fig 4.17), posing the question whether the dip was caused by the superposition of a very broad absorption band covering the whole explored UV region (with the shape of the TA at long delays) and a stimulated emission that decays in 30 ps. This would imply however, that the fluorescent state (^1L_a in the case of ethanol, according to the model presented in sec. 4.2) decays in 30 ps and that the TA occurring at larger delays originates from photoproducts other than indole, that do not come from photoionization and do not fluoresce significantly. For this reason the whole hypothesis seems not plausible.

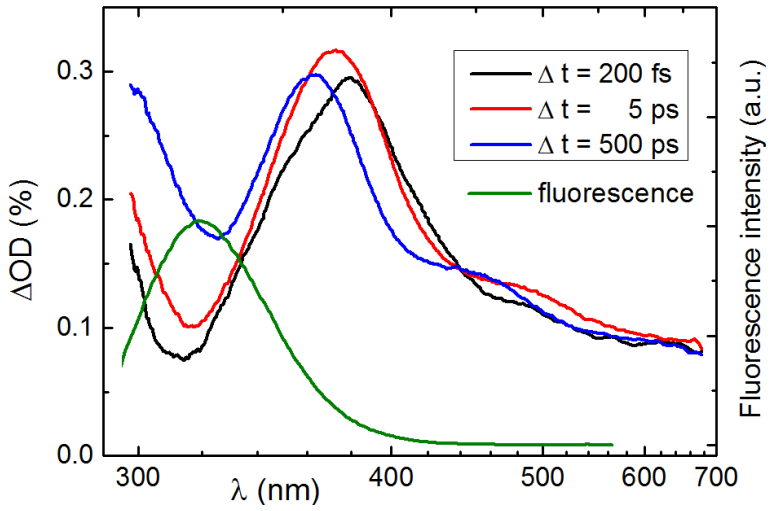

Fig 4.17 TA signal of indole in ethanol at different time delays, which clearly show the shift of the band at 370 nm but also the correspondence of the dip in the absorption with the fluorescence spectrum, suggesting a possible contribution of stimulated emission.

- a weak absorption in the visible, which appears immediately after the excitation and shows no dynamics on the investigated time scale. The absorption decreases slowly as the wavelength increases, probably due to the overlap with the band at 363 nm and

with the component described in the next point. A nearly flat absorption component all across the visible can be then reasonably assumed.

- a shoulder at about 420 nm in the shifting absorption band, whose signature is revealed by the DADS, as shown in Fig 4.18. This absorption band rises with (4 ± 1) ns and decays with a longer time constant. For this reason, we can confidently identify in this band the signature of indole triplet state, whose absorption at 430 nm is documented in literature [Kle81], where intersystem crossing is accounted as a decay pathway. The global analysis detects also a decay of the band at 300 nm with the 4 ns time constant, but since a significant part of the band extends in the UV beyond the detected range and the investigated time delays go only up to 1.6 ns, this evidence cannot be fully trusted.

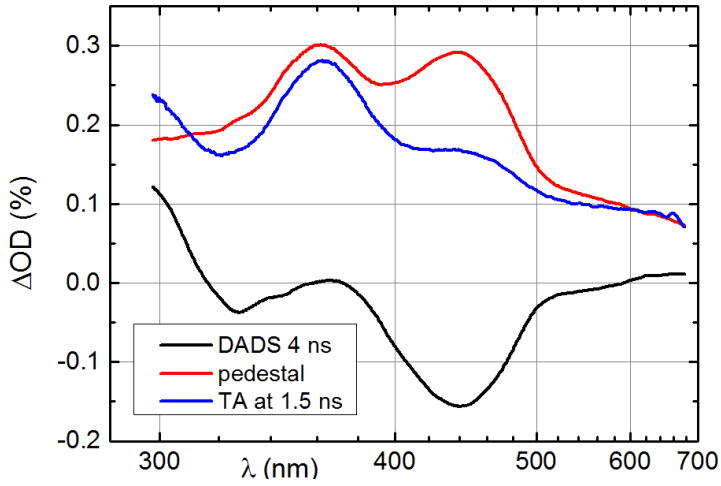

Fig 4.18 TA signal recorded 1.5 ns after excitation and long time DADS of indole in ethanol. The negative band of the black curve between 400 and 500 nm might represent the rise with ~ 4 ns of the absorption from the triplet state.

Much less dynamics is shown by the TA of indole in cyclohexane (see Fig 4.19), where photoionization does not occur [Per76]. The cyclohexane solution turned out to yield quite an unstable liquid jet with respect to the others, which made the signal very noisy. In the spectrum only a very broad absorption band centred at 370 nm is to recognize. No other dynamics but an overall (2 ± 1) ns decay can be inferred, so, as expected from a non polar environment, the signal shows no band shifts of the excited state absorption, which can be assigned to the ^1L_b state.

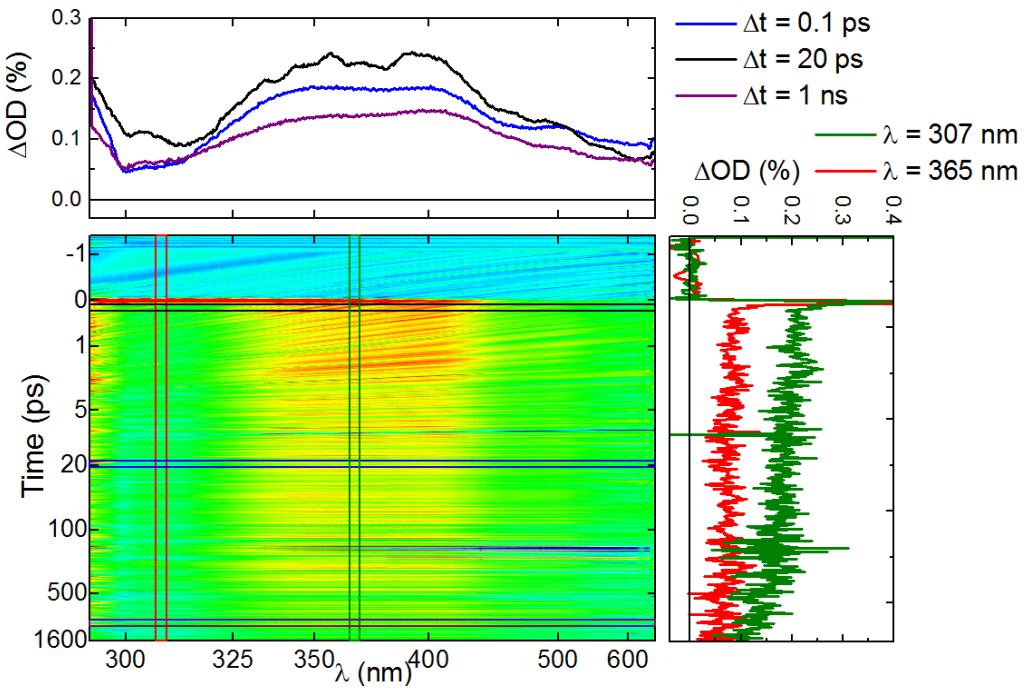

Fig 4.19 TA spectrum and profiles of indole in cyclohexane (15mM) after excitation at 272 nm.

4.5 Discussion

Pump-probe experiments to detect the TA of indole solutions in water, ethanol and cyclohexane have been performed. Band shifts to the blue have been detected for the polar solvents water and ethanol, with different magnitudes, probably due to the different polarity of the solvents. The state reversal happens right after photoexcitation and the detected shift is due to further relaxation of the band, corresponding to reorganization of solvent molecules. Proof of that is the correspondence of the time constants resulting from the fit of the band shift in ethanol (~ 4 ps and 35 ps) with those of solvation in ethanol (5.03 ps and 29.6 ps) reported in literature [Hor95]. The shifting band can be identified with the ESA from the ^1L_a state of indole as well as from its radicals. The involvement of the indole neutral radical in the de-excitation process of indole in water has been completely excluded [Biz04] or at least limited as product of the protonation of the cation, occurring microseconds after excitation [Peo99]. Nevertheless, Pernot and Lindqvist [Per76] detected its signature after the photoexcitation of indole in cyclohexane, in conditions where no photoionization takes place. They interpreted its formation through direct dissociation from indole excited singlet state,

not involving thus the production of solvated electrons, and claimed that such process may occur also in aqueous solution, so that we cannot exclude it from the analysis.

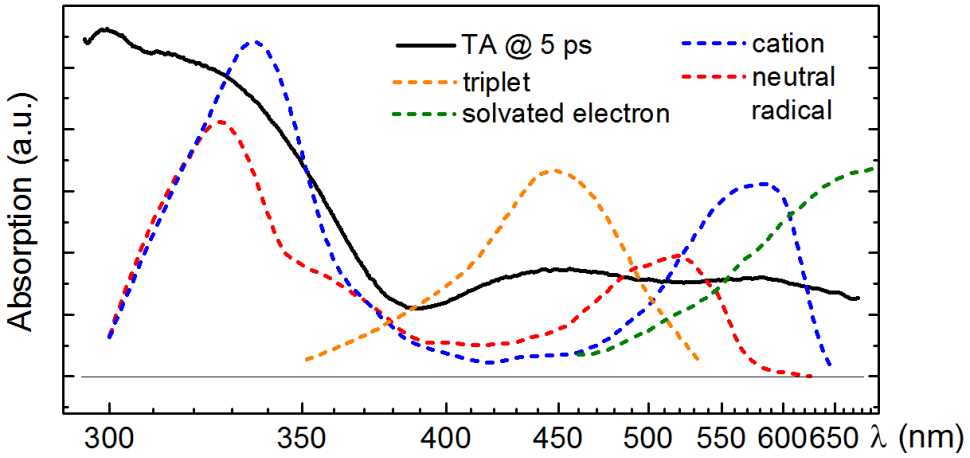

Fig 4.20 TA spectrum of indole in water 5 ps after excitation and the various species in aqueous solution that may take part in the photodynamics (with exception of indole excited molecule) taken from literature: indole triplet [Ben 74], indole radicals [Jov92] and solvated electrons [Biz04]. Spectra are differently scaled.

Fig 4.20 shows a comparison between the TA of indole in water 5 ps after the excitation and the absorption spectra of indole radicals, indole triplet and solvated electrons. All these species may contribute to the TA, together with indole excited molecule, the spectrum of which has not been found in literature. Biziak suggested that it should correspond to the TA spectrum of indole in ethanol following excitation below the photoionization threshold, as in our case. A quick look at the spectra in the two solvents shows the shifting absorption band at 360 nm in ethanol corresponds to a dip in the absorption in water. This means that, even though the spectrum in ethanol did represent the absorption of the sole excited indole molecules, this same spectrum would appear shifted (or even distorted) in water, due to the different solvent polarity. The main issues in the interpretation of this TA are the band at 300 nm, which does not belong to any of the spectra from literature but is present, with a peculiar temporal behaviour, also in the spectrum in ethanol, and the surprisingly low absorption from the solvated electrons. The molar extinction coefficient of the solvated electrons in the red is in fact particularly high ($\varepsilon(670nm) = 17500\ M^{-1}\ cm^{-1}$ [Crc91]); the signal from the electrons should be equally weighted as the indole radical cation, since they are produced together and in equal number in the photoionization process, and if it had to be scaled in order to fit our signal in the red, the cation absorption, which is weaker ($\varepsilon(330nm) = 5000\ M^{-1}\ cm^{-1}$ [Jov92])

would be barely detectable in the region of the shifting band and could not fit the signal. The effective production of solvated electrons is questioned.

It is worth mentioning at this point that our indole sample has been analyzed through NMR, gas chromatography and high performance liquid chromatography and was found to be pure at 99.6%.

Private communication with the work group of Stephen E. Bradforth at the University of Southern California confirmed similar results to ours for the TA of indole in water, measured in a liquid jet [Tau03]. They detected a band at 300 nm and a rather flat signal throughout the visible. They also performed pump-probe experiments with the addition of scavenging agents for the solvated electrons and they saw a decrease in the signal, meaning that photoionization did actually take place.

Another result of our measurements is the independence of the TA signal on the excitation wavelength in the range from 272 nm to 292 nm, i.e. either above and below the reported photoionization threshold at 285 nm. This might lead to the conclusion that no photoionization has been achieved at all or that the threshold is not correct; in a recent work Katoh measured indeed the photoionization quantum yield using the TA after excitation at 290 nm [Kat07]. This independence, however, is mirrored by the continuous wave fluorescence spectra, whose shape does not depend on the excitation energy (see Fig 4.21a), meaning that fluorescence emission always happens from the same excited state, namely the ^1L_a state. If above a certain energy photoionization took place, than an additional decay channel would be available and the fluorescence quantum yield would decrease. We tried to estimate the behaviour of this yield by dividing the fluorescence excitation spectrum by the absorption spectrum. The ratio has then been scaled to the value of 0.28 at 265 nm found in literature [Kle81], the result is shown in Fig 4.21b.

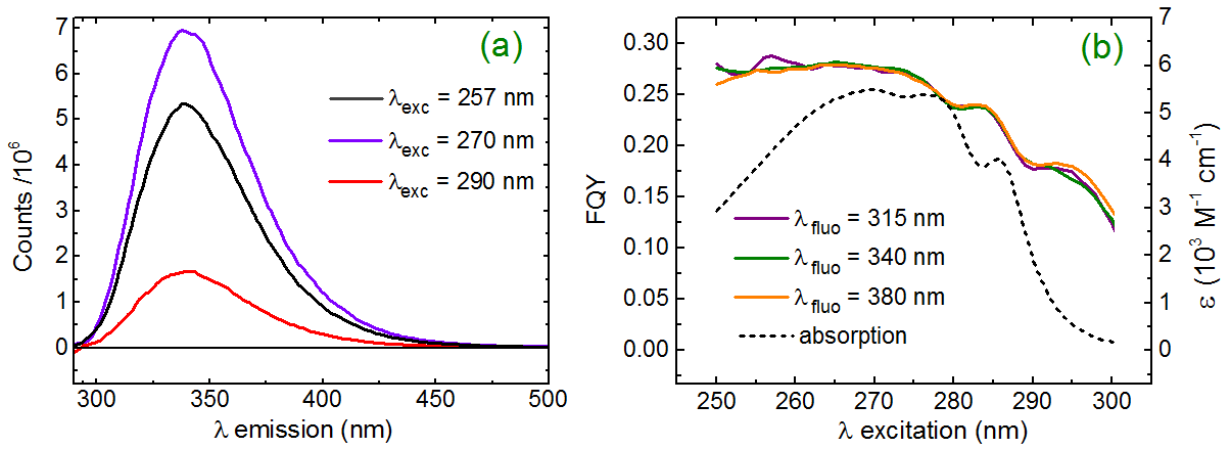

Fig 4.21 (a) Fluorescence emission of indole in water, independent on the excitation wavelength. (b) Dependence of fluorescence of indole in water on excitation, obtained as the ratio between fluorescence excitation spectrum and absorption spectrum. Data courtesy of Roland Wilken.

The fluorescence quantum yield does not get smaller at higher energies; on the contrary, it increases up to 275 nm, and remains then constant at shorter wavelengths. This raises the question about the behaviour of the quantum yield of the other decay processes that may be involved, namely internal conversion to the ground state and intersystem crossing to the triplet state, and moreover the involvement of the ^1L_b state, from which no fluorescence takes place in water but seems to experience strong vibronic coupling with ^1L_a state [Bra10, Kue10]. Katoh measured photoionization quantum yield and found it to be constant between 310 and 250 nm at the value of 0.2 and then to increase at lower wavelengths up to the value of 0.26 [Kat07] and he suggested that this increase should be ascribed to the contribution of a B_b state. He also stressed the conclusion that the photoionization quantum yield via the ^1L_a state is the same as that via the ^1L_b state and, following evidence from [Jal04], he decomposed indole absorption spectrum into ^1L_a and ^1L_b absorption bands by exploiting the assumption that the spectrum of ^1L_a state can be modelled with a single Gaussian function. The result is displayed in Fig 4.22 and shows how the two components significantly overlap in the lower energy region, meaning that they cannot be separately excited, at least not with the setup we have been using for pump-probe measurements. Similar results were obtained in propylene glycol by Valeur and Weber [Val77].

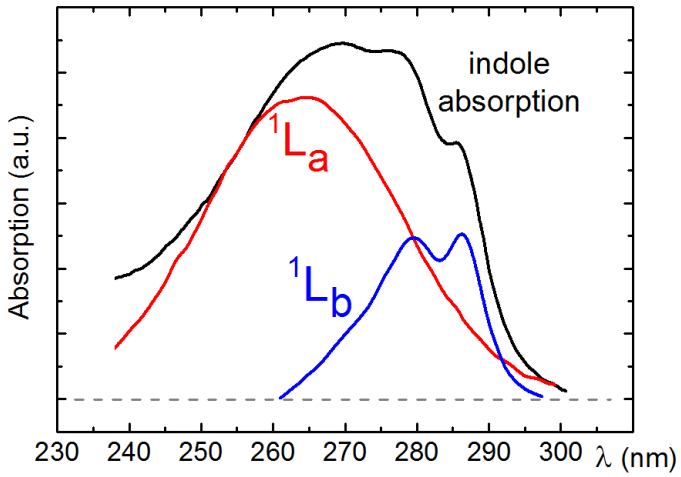

Fig 4.22 Decomposition of indole absorption spectrum into the two lowest excited ππ* states ^1L_a and ^1L_b, according to ref. [Kat07].

Comparing this last graph with the calculated behaviour of the fluorescence quantum yield in Fig 4.21b we could argue that the latter is influenced by the population of the ^1L_b state, i.e. that this state has a higher probability than the ^1L_a to undergo radiationless decay.

Another remark from Katoh's work is that the generation of solvated electrons does not happen through direct photoionization, but through an electron transfer from a short-lived intermediate state, most likely the lowest $^1\pi\sigma^*$ which has a repulsive potential energy profile over the NH bond coordinate and crosses both the lowest $\pi\pi^*$ states [Sob02], to pre-existing trap sites in the solvent, formed by density fluctuations of water.

We did not find any sign of recombination of the electrons up to 1.5 ns after excitation, i.e. the TA signal in the red remained constant, so the question about the existence of an energy barrier for recombination [Peo99] and whether the latter proceeds at diffusion limit or not remains open [Ste00].

5. Conclusions and outlook

In this work, pump-probe spectroscopy and time resolved fluorescence have been applied to the study of the ultrafast photodynamics of the pyrene and indole molecules in solution.

The temporal analysis of the ground-state bleach recovery of pyrene led to the conclusion that a significant fraction of pyrene molecules gets excited some picoseconds after the light-induced excitation of the sample. Starting from this evidence we proposed a new model to interpret the photodynamics of pyrene in solution. This model employs the idea of loosely bound dimers and reinterprets the roles of the pyrene excimer and charge-transfer states, but at the same time it adopts the usual mathematical frame for the time behaviour of the population of the states and for the dependence on pyrene concentration. The model is based on demanding hypotheses (like the fact that pyrene could exist in solution only as a preassociated dimer) that still need to be properly supported by experimental evidence. The ground-state bleach has to be object of deeper investigation in order to confirm its relaxation features and to study its dependence on the solvent nature, which is expected to have a role in a preassociation mechanism. The involvement of the triplet state has to be cleared too, since the evidence collected in this work was not sufficient to unravel its formation mechanism. The correspondence between the time constants estimated from the transient absorption experiments and from the time-resolved fluorescence was not systematic, improvements on the degassing procedure will therefore be needed. An anomalous additional time constant has been found in the decay of the fluorescence emission of pyrene at 390 nm after direct excitation of the S_1 state. This was interpreted as the signature of a second species in solution. Evidence of the degradation of pyrene upon irradiation in the form of the variation of the steady-state absorption spectrum of the solution was collected, and the spectrum of the photoproduct was extracted. At the moment of the writing of this thesis, thorough experiments are being performed in order to identify the photoproduct and to verify the connection between this and the anomalous fast component of the fluorescence decay.

A setup for the measurement of transient absorption from a solution flowing in a liquid jet has been built and used in order to study indole. Signatures of a state reversal of the two lowest excited states in polar solvents have been detected, as well as an absorption band at 300 nm which was not reported in literature. The absorption from the solvated electron was found to be particularly weak. An analysis of the fluorescence quantum yield suggests that the two $\pi\pi^*$

states may have different probabilities to undergo a radiationless decay. This work was intended as a preliminary investigation on indole dynamics and will proceed with further experiments extending the spectral range of the probe light either in the UV region, in order to study the band at 300 nm and the GSB recovery (which, as shown in the case of pyrene, can offer great insight into population dynamics), and in the NIR, where the signal of the solvated electrons is predominant. The dynamics on the nanosecond time scale will also be investigated, with attention to the recombination process and with the employment of quenchers in order to perform excitation dependence studies of the photoionization quantum yield.

Bibliography

[Aal59] W.I. Aalbersberg, G.J. Hoijtink, E.L. Mackor, W.P. Weijland, *The formation of hydrocarbon positive ions in strong proton donors*, J. Chem. Soc., 1959, 3049.

[Acr02] W.E. Acree, M.H. Abraham, *Solubility predictions for crystalline polycyclic aromatic hydrocarbons (PAHs) dissolved in organic solvents based upon Abraham general salvation model*, 2002, Fluid Phase Equilibria, **201**, 245.

[And92] R. Andriessen, M. Ameloot, N. Boens, F.C. De Schryver, *Non a Priori Analysis of Fluorescence Decay Surfaces of Excited-State Processes. 3. Intermolecular Excimer Formation of Pyrene Quenched by Iodomethane*, J. Phys. Chem., 1992, **96**, 314.

[Azu64] T. Azumi, S.P. McGlynn, *Energy of excimer luminescence. I. A reconsideration of excimer processes*, J. Chem. Phys., 1964, **41**, 3131.

[Azu64b] T. Azumi, A.T. Armstrong, S.P. McGlynn, *Energy of excimer luminescence. II. Configuration interaction between molecular exciton states and resonance states*, J. Chem. Phys., 1964, **41**, 3839.

[Bai11] G. Bains, A.B. Patel, V. Narayanaswami, *Pyrene: A Probe to Study Protein Conformation and Conformational Changes*, Molecules, 2011, **16**, 7909.

[Bee85] J. M. Beechem, L. Brand, *Time-resolved fluorescence of proteins*, Ann. Rev. Biochem., 1985, **54**, 43.

[Ben74] D.V. Bent, E. Hayon, *Excited state chemistry of aromatic amino acids and related peptides. III. Tryptophan*, J. Am. Chem. Soc., 1975, **97**, 2612.

[Ber10] M. Y. Berezin and S. Achilefu, *Fluorescence lifetime measurements and biological imaging*, Chem. Rev., 2010, 110, 2641–2684.

[Ber80] A. Bernas, D. Grand, E. Arnouyal, *Photoionization of solutes and conduction band edge of solvents. Indole in water and alcohols*, J. Phys. Chem., 1980, **84**, 1259.

[Bir63] J. B. Birks, D. J. Dyson, I. H. Munro, *'Excimer' fluorescence II . Lifetime studies of pyrene solutions*, Proc. R. Soc. London, Ser. A, 1963, **274**, 552-564.

[Bir70] J. B. Birks, *Photophysics of Aromatic Molecules*, Wiley-Interscience, London, 1970.

[Bir75] J. B. Birks, *Excimers*, Rep. Prog. Phys., 1975, **38**, 903.

[Biz04] T. Bizjak, *Ultrafast photoinduced intra- and intermolecular charge transfer and salvation*, Dissertation LMU Munich, 2004.

[Bra10] C. Brand, J. Küpper, D.W. Pratt, W.L. Meerts, D. Krügler, J. Tatchen, M. Schmitt, *Vibronic coupling in indole: I. Theoretical description of the ^1L_a–^1L_b interaction and the electronic spectrum*, Phys. Chem. Chem. Phys., 2010, **12**, 4968.

[Cal97] P.R. Callis, *L-1(a) and L-1(b) transitions of tryptophan: Applications of theory and experimental observations to fluorescence of proteins*, Methods Enzymol., 1997, **278**, 113.

[Cer03] G. Cerullo, S. De Silvestri, *Ultrafast optical parametric amplifiers*, Rev. Sci. Instrum., 2003, **74**, 1.

[Che98] Y. Chen, M.D. Barkley, *Toward understanding tryptophan fluorescence in proteins*, Biochem., 1998, **37**, 9976.

[Crc91] CRC Handbook of Radiation Chemistry, CRC Press, Boca Raton, FL, 1991.

[Dei71] T. Deinum, C.J. Werkhoven, J. Langelaar, R.P.H. Rettschnick, J.D.W. Voorst, *Intermediate strong coupling and vibrational redistribution effects in the S_2 emission of pyrene*, Chem. Phys. Lett., 1971, **12**, 189.

[Fer65] J. Ferguson, *Excited dimer (excimer) luminescence from aromatic molecules in crystalline cyclohexane*, J. Chem. Physics, 1965, **43**, 306.

[Fig11] T.M. Figueira-Duarte and K. Müllen, *Pyrene-based materials for organic electronics*, Chem. Rev., 2011, 111, 7260–7314.

[Fit06] P. Fita, E. Luzina, T. Dziembowska, Cz. Radzewicz, A. Grabowska, *Chemistry, photophysics, and ultrafast kinetics of two structurally related Schiff bases containing the naphthalene or quinoline ring*, J. Chem. Phys., 2006, **125**, 184508.

[Foe55] T. Förster and K. Kasper, *Ein Konzentrationsumschlag der Fluoreszenz des Pyrenes*, Z. Electrochem., 1955, **59**, 976–980.

[Gal95] G.M. Gale, M. Cavallari, T.J. Driscoll, F. Hache, *Sub-20-fs tunable pulses in the visible from an 82-MHz optical parametric oscillator*, Opt. Lett., 1995, **20**, 1562.

[Gra79] D. Grand, A. Bernas, E. Amouyal, *Photoionization of aqueous indole; conduction band edge and energy gap in liquid water*, Chem. Phys., 1979, **44**, 73.

[Gre73] K.H. Grellmann, A.R. Watkins, *Photoionization of pyrene in polar solvents. The role of the triplet state*, J. Am. Chem. Soc., 1973, **95**, 983.

[Gri04] S. Grimme, *Accurate description of the van der Waals complexes by density functional theory including empirical corrections*, J. Comput. Chem., 2004, **25**, 1463.

[Han13] A. D. Hanlon, B. H. Milosavljevic, *Appropriate excitation wavelenght removes obfuscation from pyrene excimer kinetics and mechanism studies*, Photochem. Photobiol. Sci., 2013, **12**, 787-797.

[Hei69] W. Heinzelmann, H. Labhart, *Triplet-triplet spectra and triplet quantum yields of some aromatic hydrocarbons in liquid solution*, Chem. Phys. Lett., 1969, **4**, 20.

[Hir89] Y. Hirata, N. Murata, Y. Tanioka, N. Mataga, *Dynamic behaviour of solvated electrons produced by photoionization od indole and tryptophan in several polar solvents*, J. Phys. Chem. 1989, **93**, 4527.

[Hue08] R. Huenerbein and S. Grimme, *Time-dependent density functional study of excimers and exciplexes of organic molecules*, Chem. Phys., 2008, **343**, 362–371.

[Kas50] M. Kasha, *Characterisation of electronic transitions in complex molecules*, Discussions of the Faraday Society, 1950, **9**, 14.

[Kat07] R. Katoh, *Dependence of photoionization quantum yield of indole and tryptophan in water on excitation wavelength*, J. Photochem. Photobiol. A, 2007, **189**, 211.

[Kha01] O.A. Khakhel, *Absorption spectra of pyrene aggregates in saturated solutions*, J. Appl. Spec., 2001, **68**, 280.

[Kle81] R. Klein, I. Tatischeff, M. Bazin, R. Santus, *Photophysics of indole. Comparative study of quenching, solvent, and temperature effects by laser flash photolysis and fluorescence*, J. Phys. Chem., 1981, **85**, 670.

[Kre13] N. Krebs, *New insights for femtosecond spectroscopy*, Dissertation, LMU Munich, 2013.

[Kue10] J. Küpper, D.W. Pratt, W.L. Meerts, C. Brand, J. Tatchen, M. Schmitt, *Vibronic coupling in indole: II. Investigation of the* ^1L_a - ^1L_b *interaction using rotationally resolved electronic spectroscopy*, Phys. Chem. Chem. Phys., 2010, **12**, 4980.

[Lai06] S. Laimgruber, H. Schachenmayr, B. Schmidt, W. Zinth, P. Gilch, *A femtosecond stimulated raman spectrograph for the near ultraviolet*, Appl. Phys. B, 2006, **85**, 557.

[Lak06] J.R. Lakowicz, *Principles of Fluorescence Spectroscopy*, Springer, 2006.

[Lam86] H. Lami, N. Glasser, *Indole's solvatochromism revisited*, J. Chem. Phys., 1986, **84**, 597.

[Lip04] H. Lippert, H.-H. Ritze, I.V. Hertel, W. Radloff, *Femtosecond time-resolved analysis of the photophysics of the indole molecule*, Chem. Phys. Lett., 2004, **398**, 526.

[Lor02] M. Lorenc, M. Ziolek, R. Naskrecki, J. Karolczak, J. Kubicki, A. Maciejewski, *Artifacts in femtosecond transient absorption spectroscopy*, Appl. Phys. B, 2002, **74**, 19-27.

[Mai10] L. Maisenbacher, *Ultraschnelle initialdynamik des photoinduzierten bindungsbruchs im diphenylmethylchlorid*, Bachelor thesis, LMU Munich, 2010.

[Mar92] J.M.G. Martinho, J.P. Farinha, M.N. Berberan-Santos, J. Duhamel and M.A. Winnik, *Test of a model for reversible excimer kinetics: Pyrene in cyclohexanol*, J. Chem. Phys., 1992, **96**, 8143.

[Meg09] U. Megerle, I. Pugliesi, C. Schriever, C.F. Sailer and E. Riedle, *Sub-50 fs broadband absorption spectroscopy with tunable excitation: putting the analysis of ultrafast molecular dynamics on solid ground*, Appl. Phys. B, 2009, **96**, 215-231.

[Meg11] U. Megerle, M. Wenninger, R. Kutta, R. Lechner, B. König, B. Dick, E. Riedle, *Unraveling the flavin-catalyzed photooxidation of benzylic alcohol with transient absorption spectroscopy from sub-pico- to microseconds*, Phys. Chem. Chem. Phys., 2011, **13**, 8869.

[Meg11b] U. Megerle, *Photoinduced molecular dynamics in increasingly complex systems: From ultrafast transient absorption spectroscopy to nanoscopic models*, Dissertation, LMU Munich, 2011.

[Mon12] R. Montero, A.P. Conde, V. Ovejas, F. Castaño, A. Longarte, *Ultrafast photophysics of the isolated indole molecule*, J. Phys. Chem. A, 2012, **116**, 2698.

[Mur64] J.N. Murrell, J. Tanaka, *The theory of the electronic spectra of aromatic hydrocarbon dimers*, J. Mol. Phys, 1964, **7**, 363.

[Neu99] F.V.R. Neuwahl, P. Foggi, *Direct observation of S_2-S_1 internal conversion in pyrene by femtosecond transient absorption*, Laser Chem., 1999, **19**, 375.

[Par06] Y.H. Park, B.-S. Cheong, *Theoretical investigation of electronic structures of the*

ground and excited states of pyrene and its derivatives, Cur. Appl. Phys., 2006, **6**, 700.

[Par09] W.W. Parson, *Modern Optical Spectroscopy*, Springer, 2009.

[Par61] C.A. Parker, C.G. Hatchard, *Lifetime of the pyrene dimer*, Nature, 1961, **190**, 165.

[Pen02] P. Somerharju, *Pyrene-labeled lipids as tools in membrane biophysics and cell biology*, Chem. Phys. Lipids, 2002, **116**, 57.

[Per76] C. Pernot, L. Lindqvist, Laser *photolysis of indole in cyclohexane*, J. Photochem., 1976/77, **6**, 215.

[Pla49]J.R. Platt, *Classification of spectra of cata-condensed hydrocarbons*, J. Chem. Phys., 1949, **17**, 484.

[Ras01] M. Rasmusson, A. N. Tarnovsky, E. Åkesson, V. Sundström, *On the use of two-photon absoprtion for determination of femtosecond pump-probe cross-correlation functions*, Chem. Phys. Lett., 2001, **335**, 201.

[Ray03] M. Raytchev, E. Pandurski, I. Buchvarov, C. Modrakowski, and T. Fiebig, *Bichromophoric Interactions and Time-Dependent Excited State Mixing in Pyrene Derivatives. A Femtosecond Broad-Band Pump-Probe Study*, J. Phys. Chem. A, 2003, **107**, 4592.

[Rei94] C. Reichardt, *Solvatochromic Dyes as Solvent Polarity Indicators*, Chem. Rev., 1994, **94**, 2319.

[Rie00] E. Riedle, M. Beutter, S. Lochbrunner, J. Piel, S. Schenkl, S. Spörlein, W. Zinth, *Generation of 10 to 50 fs pulses tunable through all of the visible and the NIR*, Appl. Phys. B: Lasers Opt., 2000, **70**, 457.

[Rie13] E. Riedle, M. Bradler, M. Wenninger, C.F. Sailer and I. Pugliesi, *Electronic transient spectroscopy from deep UV to the NIR: unambiguous disentanglement of complex processes*, Faraday Discuss., 2013, **163**, 139-158.

[Sai97] F. Saito, S. Tobita, H. Shizuka, Photoionization mechanism of aniline derivatives in aqueous solution studied by laser flash photolysis, J. Photochem. Photobiol. A, 1997, **106**, 119.

[Sch05] S. Schenkl, F. Van Mourik, G. van der Zwan, S. Haacke, M. Chergui, *Probing the ultrafast charge translocation of photoexcited retinal in bacteriorhodopsin*, Science, 2005, **309**, 917.

[Sha10] D. Sharma, J. Leonard, S. Haacke, *Ultrafast excited-state dynamics of tryptophan in water observed by transient absorption spectroscopy*, Chem. Phys. Lett., 2010, **489**, 99.

[Shi07] J. Shirdel, *Photo-physical characterization of flavin-pyrene-phenothiazine molecular photonic complexes*, Dissertation, Universität Regensburg, 2007.

[Shi11] S. Shirai, S. Iwata, T. Tani and S. Inagaki, *Ab initio studies of aromatic excimers using multiconfiguration quasidegenerate perturbation theory*, J. Phys. Chem. A, 2011, 115, 7687–7699.

[Sob02] A.L. Sobolewski, W. Domcke, C. Dedonder-Lardeux, C. Jouvet, *Excited-state hydrogen detachment and hydrogen transfer driven by repulsive $^1\pi\sigma^*$ states: A new paradigm for nonradiative decay in aromatic biomolecules*, Phys. Chem. Chem. Phys., 2002, **4**, 1093.

[Sob99] A.L. Sobolewski, W. Domcke, *Ab initio investigations on the photophysics of indole*, Chem. Phys. Lett., 1999, **315**, 293.

[Ste00] K.L. Stevenson, G.A. Papadantonakis, P.R. LeBreton, *Nanosecond UV laser photoionization of aqueous tryptophan: temperature dependence of quantum yield, mechanism, and kinetics of hydrated electron decay*, J. Photochem. Photobiol. A, 2000, **133**, 159.

[Ste60] B. Stevens and E. Hutton, *Radiative life-time of the pyrene dimer and the possible role of excited dimers in energy transfer processes*, Nature, 1960, **186**, 1045–1046.

[Sto04] I.H.M. van Stokkum, D.S. Larsen, R. van Grondelle, *Global and target analysis of time-resolved spectra*, Biochem. Biophys. Acta, 2004, **1657**, 82.

[Sza80] A.G. Szabo, D.M. Rayner, *Fluorescence decay of tryptophan conformers in aqueous solution*, J. Am. Chem. Soc., 1980, **102**, 554.

[Tau03] M.J. Tauber, R.A. Mathies, X. Chen, S.E. Bradforth, *Flowing liquid sample jet for resonance Raman and ultrafast optical spectroscopy*, Rev. Sci. Instrum., 2003, **74**, 4958.

[Val77] B. Valeur, G. Weber, *Resolution of the fluorescence excitation spectrum of indole into the ^1L_a and ^1L_b excitation bands*, Photochem. Photobiol., 1977, **25**, 441.

[Wal67] M.S. Walker, T.W. Bednar, R. Lumry, *Exciplex studies. II. Indole and indole derivatives*, J. Chem. Phys., 1967, **47**, 1020.

[Wik01] http://en.wikipedia.org/wiki/Solvent#Properties_table_of_common_solvents

[Wil97] T. Wilhelm, J. Piel, E. Riedle, Sub-20-fs pulses tunable across the visible from a blue-pumped single-pass noncollinear parametric converter, Opt. Lett., 1997, **22**, 1494.

[Win93] F.M. Winnik, *Photophysics of Preassociated Pyrenes in Aqueous Polymer Solutions and in Other Organized Media*, Chem. Rev., 1993, **93**, 587.

[Zha06] L. Zhang, Y. Tao, W. Qiu, L. Wang, D. Zhong, *Femtosecond studies of tryptophan fluorescence dynamics in proteins: local solvation and electronic quenching*, J. Phys. Chem. B, 2006, **110**, 18097.

Acknowledgments

This thesis is the outcome of ten months of work carried out at the facilities of the BioMolecular Optics chair at the LMU in Munich. I owe to many people the overcoming of this task.

My gratitude goes in the first place to Prof. Eberhard Ridle, which gave me the possibility to work at BMO, joining thus a outstanding staff and a stimulating environment.

A huge thank you goes to my supervisor and friend Igor Pugliesi, for having been always at my side during this work, for all the training he gave me, for the advice about life and career, and for the innumerable funny moments and conversations on the edge between seriousness and hilarity that we had together.

Many thanks also to Bastian Baudisch, for his help with the fluorescence measurements and for the cheerful atmosphere he can create around himself, to Roland Wilken, for all the instructive conversations and the patient training with the NOPA, to Qi Hu and Philipp Hummel, for the pleasant time and discussions we had together, and to all the colleges at BMO, Max, Andreas, Immanuel, Sebastian, Rudi, Matthias and Nils.

I would like to thank my Italian supervisor Prof. Cinzia Sada, who trusted my capabilities from the first meeting and always supported me with help and advice.

Endless gratitude and affection goes to Gabi, who gave me house, home and family in a foreign land, which was the best I could ask for.

A special thanks goes then to my family, that gave me the possibility to attend my studies, and moreover never ceased to love me after all these years, but still cares about me every day double than the previous one.